JACS Au
AN OPEN ACCESS JOURNAL OF THE AMERICAN CHEMICAL SOCIETY

pubs.acs.org/jacsau

Article

Advanced Molecular Tweezers with Lipid Anchors against SARS-CoV-2 and Other Respiratory Viruses

Tatjana Weil, Abbna Kirupakaran,° My-Hue Le,° Philipp Rebmann,° Joel Mieres-Perez, Leila Issmail, Carina Conzelmann, Janis A. Müller, Lena Rauch, Andrea Gilg, Lukas Wettstein, Rüdiger Groß, Clarissa Read, Tim Bergner, Sandra Axberg Pålsson, Nadja Uhlig, Valentina Eberlein, Heike Wöll, Frank-Gerrit Klärner, Steffen Stenger, Beate M. Kümmerer, Hendrik Streeck, Giorgio Fois, Manfred Frick, Peter Braubach, Anna-Lena Spetz, Thomas Grunwald, James Shorter, Elsa Sanchez-Garcia,* Thomas Schrader,* and Jan Münch*

Cite This: https://doi.org/10.1021/jacsau.2c00220

Read Online

ACCESS | Metrics & More | Article Recommendations | Supporting Information

ABSTRACT: The COVID-19 pandemic caused by SARS-CoV-2 presents a global health emergency. Therapeutic options against SARS-CoV-2 are still very limited but urgently required. Molecular tweezers are supramolecular agents that destabilize the envelope of viruses resulting in a loss of viral infectivity. Here, we show that first-generation tweezers, CLR01 and CLR05, disrupt the SARS-CoV-2 envelope and abrogate viral infectivity. To increase the antiviral activity, a series of 34 advanced molecular tweezers were synthesized by insertion of aliphatic or aromatic ester groups on the phosphate moieties of the parent molecule CLR01. A structure-activity relationship study enabled the identification of tweezers with a markedly enhanced ability to destroy lipid bilayers and to suppress SARS-CoV-2 infection. Selected tweezer derivatives retain activity in airway mucus and inactivate the SARS-CoV-2 wildtype and variants of concern as well as respiratory syncytial, influenza, and measles viruses. Moreover, inhibitory activity of advanced tweezers against respiratory syncytial virus and SARS-CoV-2 was confirmed in mice. Thus, potentiated tweezers are broad-spectrum antiviral agents with great prospects for clinical development to combat highly pathogenic viruses.

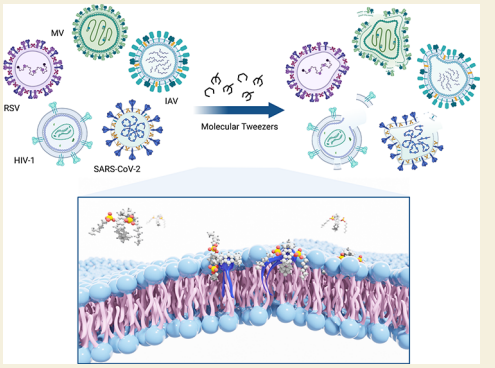

KEYWORDS: *broad-spectrum antivirals, SARS-CoV-2, RSV, molecular tweezers, respiratory viruses*

Downloaded via 68.81.196.217 on September 7, 2022 at 14:32:27 (UTC).
See https://pubs.acs.org/sharingguidelines for options on how to legitimately share published articles.

The coronavirus disease 2019 (COVID-19) pandemic is a tremendous threat to humans and global socioeconomics. The causative agent of COVID-19, the severe acute respiratory syndrome coronavirus 2 (SARS-CoV-2), was first described in late 2019 in Wuhan, China, and since then spread globally. In June 2022, the WHO reported ~530 million confirmed infections and ~6.2 million deaths due to COVID-19. There are thousands of clinical trials investigating treatments and preventative measures for the disease; however, only a few antiviral drugs are approved to date including remdesivir, with only a modest clinical benefit, and PAXLOVID, which treatment is only authorized for patients requiring hospitalization due to severe or critical COVID-19.[1,2] Other compounds, in particular therapeutic antibodies, received emergency use authorization in some countries but showed variable efficacy in hospitalized patients.[3] The rollout of mass vaccination campaigns in the end of 2020 is expected to substantially reduce incidence of severe disease, morbidity, and mortality and may result in "herd immunity".[4,5] Vaccination success may, however, be compromised by the emergence of viral variants of concern (VOC) that escape immunity,[6,7] exhibit a multiplicative transmissibility,[8,9] and cause higher case fatality rates.[10,11] In addition, widespread refusal to get vaccinated and a slow rollout of vaccines may facilitate VOC selection, raising the question of whether herd immunity can really be achieved. These troubling issues highlight the ongoing need to develop broadly protective and therapeutic intervention agents against SARS-CoV-2.

In addition to SARS-CoV-2, other emerging and re-emerging viruses with epidemic potential such as Ebola virus (EBOV), Zika virus (ZIKV), SARS-CoV, Middle East respiratory syndrome coronavirus (MERS-CoV), or new strains of influenza A virus (IAV) pose significant threats to human health due to the absence of available antiviral therapies or effective vaccines. These viruses, as well as other widespread

Received: April 7, 2022
Revised: July 6, 2022
Accepted: July 7, 2022

ACS Publications
© XXXX The Authors. Published by American Chemical Society

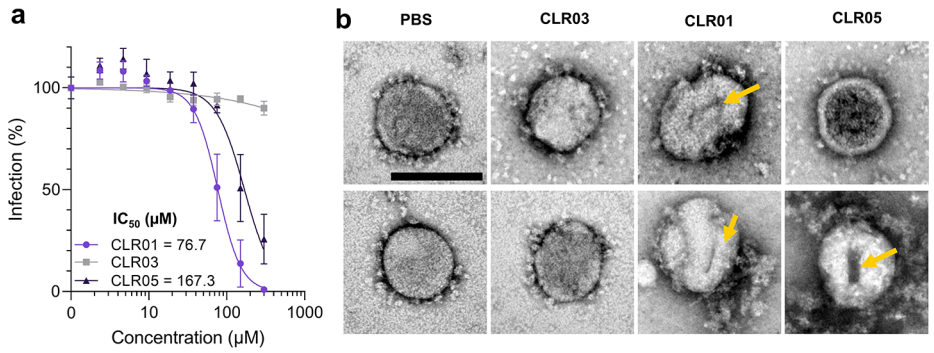

Figure 1. CLR01 and CLR05 inactivate SARS-CoV-2. (a) Tweezers suppress SARS-CoV-2 infection. SARS-CoV-2 (Wuhan) was incubated with CLR01, CLR05, or CLR03 at indicated concentrations for 2 h at 37 °C and then used to inoculate Caco2 cells. Two days later, infection rates were quantified by measuring viral S-protein using an in-cell ELISA. Values represent mean percent values normalized to mock infected controls and derived from two experiments each performed in triplicate (± SEM). (b) CLR01- and CLR05-damaged SARS-CoV-2 virions. SARS-CoV-2 (1.2×10^6 PFU/mL) was incubated with PBS or 250 μM of CLR01, CLR03, and CLR05 for 30 min at 37 °C, fixed, stained with uranyl acetate, and visualized by TEM. Scale bar = 100 nm. The yellow arrow indicates notches in the viral envelope induced by molecular tweezer treatment. For more images and quantification, see Figure S2.

viral pathogens such as respiratory syncytial virus (RSV), measles virus (MeV), herpes simplex viruses (HSV-1 and HSV-2), and human immunodeficiency virus type 1 (HIV-1), share a common feature: they are surrounded by an envelope. The envelope consists of a lipid bilayer, which is derived from cellular membranes and contains viral glycoproteins that mediate cell attachment and entry. Compounds that disrupt the lipid bilayer such as alcohols and detergents are virucidal and have been used as disinfectants for decades. More recently, it became clear that the lipid bilayer may also serve as target for labyrinthopeptins, the AH peptide, and a novel class of antiviral compounds, termed molecular tweezers.[12−15] These small molecules have a belt-like arrangement with a horseshoe-shaped cavity that enables them to bind to lipid head groups of the phospholipids in the viral envelope and subsequently insert into the lipid bilayer, which results in increased surface tension, membrane disruption, and a loss of viral infectivity.[14] Consequently, molecular tweezers CLR01 and CLR05 displayed broad antiviral activity against all enveloped viruses tested so far, including HIV-1, ZIKV, HSV-1, HSV-2, HCMV, MeV, EBOV, and IAV.[13,14,16] These broad-spectrum antiviral agents are being evaluated in preclinical studies as microbicides to prevent sexual HSV-2 and HIV-1 transmission or as prophylactic and therapeutic agents in respiratory tract infections.

More recently, in a preliminary structure-activity relationship study, we synthesized and analyzed nine CLR01 derivatives containing aliphatic ester arms and found them to be able to destroy liposomes and to inhibit HIV-1 infection more efficiently than the parental molecule.[14] Thus, we here set out to explore whether first- and second-generation molecular tweezers may also inactivate SARS-CoV-2 and other respiratory pathogens. We found that the first-generation tweezers CLR01 and CLR05 inactivate live SARS-CoV-2 with modest antiviral activities in the high micromolar range. To improve the virucidal activity, we performed a more comprehensive systematic structure-activity relationship (SAR) study and synthesized more than 30 additional CLR01 derivatives containing additional aliphatic and aromatic ester groups to facilitate membrane binding and disruption. Most of the newly designed tweezers exhibited markedly increased antiviral activity with some even reaching the nanomolar range while retaining good selectivity indices. Biomolecular modeling confirmed that optimized tweezers interact with the viral membrane more efficiently, thereby further supporting an increased surface tension and ultimately viral membrane disruption. Finally, we show that the optimized tweezers also inactivate MeV, RSV, and IAV. Thus, potentiated tweezers are broad-spectrum antivirals that could help our fight against SARS-CoV-2 and other respiratory viruses.

RESULTS

Molecular Tweezers CLR01 and CLR05 Inactivate SARS-CoV-2

CLR01 and CLR05 (structures shown in Figure S1a) display broad antiviral activity against several enveloped viruses[12−14] and have previously been shown to inactivate lentiviral particles pseudotyped with the SARS-CoV-2 spike protein[17] with half-maximal inhibitory concentrations (IC_{50}) of 36 μM for CLR01 and 33 μM for CLR05.[14] CLR03, which is based on a truncated polycyclic backbone (Figure S1a), is unable to interact with the viral membrane[12] and did not affect pseudoparticle entry.[14] We here additionally show that none of the tested tweezers were cytotoxic at antivirally active concentrations. CLR05 shows cytotoxicity only at the highest concentrations (CC_{50} of 117 μM) (Figure S1b). The antiviral activity of CLR01 to block the SARS-CoV-2 spike pseudovirus increased over time, with the maximum inhibition observed after 5 h (Figure S1c). Furthermore, we found that IC_{50} values of CLR01 and CLR05 increased with elevated amounts of spike pseudoparticles (Figure S1d), confirming that tweezers target the viral particles.

We next determined the antiviral activity of CLR01, CLR03, and CLR05 against infectious SARS-CoV-2. For this experiment, a low dose of SARS-CoV-2 (multiplicity of infection, MOI = 0.01) was treated with the tweezers, and then, the mixtures were used for inoculation of Caco2 cells. Quantification of the viral S-protein by an in-cell ELISA showed that CLR01 and CLR05 suppressed SARS-CoV-2 infection with IC_{50} values of 77 and 167 μM, respectively, while CLR03 was inactive (Figure 1a). Complete inhibition of viral infection was achieved by ∼300 μM of CLR01, whereas the same concentration of CLR05 inhibited virus infection by ∼70% (Figure 1a).

https://doi.org/10.1021/jacsau.2c00220
JACS Au XXXX, XXX, XXX−XXX

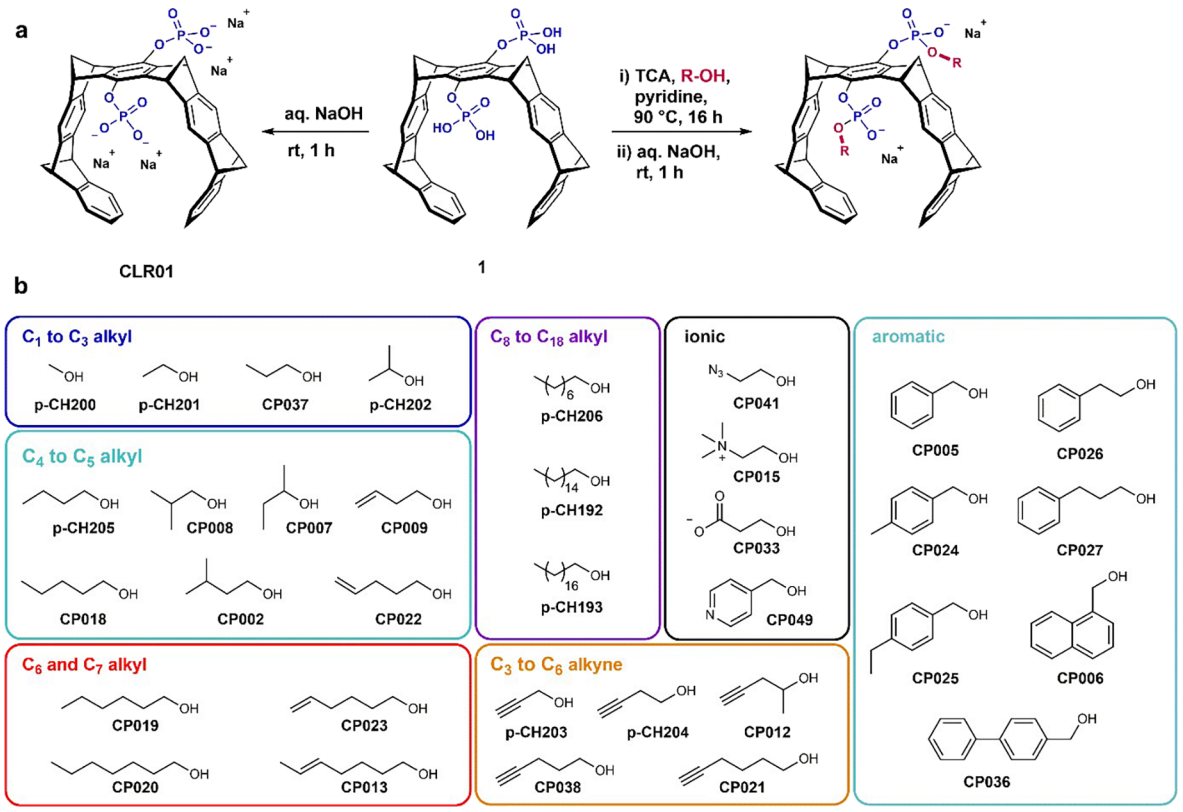

Figure 2. Synthesis of dialkyl diphosphate tweezers and overview of all new compounds in groups of similar chemical structure. (a) Conversion of the free diphosphoric acid 1 to CLR01 and TCA-mediated esterification reaction with subsequent neutralization leading to dialkyl diphosphate tweezers. (b) Overview of all ester alcohols attached to the parent tweezer CLR01, classified according to their size and chemical nature. Advanced tweezers p-CH200, p-CH201, p-CH202, p-CH203, p-CH204, p-CH205, p-CH206, p-CH192, and p-CH193 were previously reported.[14]

Transmission electron microscopy (TEM) analysis of buffer and CLR03 (inactive tweezer derivative)-treated virions revealed the presence of SARS-CoV-2 virions with a typical size of around 100 nm[18] and envelope "corona" formed by the spike peplomers (Figure 1b, Figure S2a). In contrast, the morphology of CLR01- and CLR05-treated virions was largely disrupted (Figure 1b, Figure S2a) and associated with a reduced number of clearly visible peplomers at the virion surface, envelope notches, and a loss of sphericity (Figure 1b, Figure S2b). We also observed an electron-dense material in the virion center, caused by uranyl acetate penetrating into the damaged lipid bilayer, which indicates disruption of the viral membrane upon tweezer treatment (Supplementary Movie 1). Altogether, these data show that CLR01 and CLR05 inactivate SARS-CoV-2 by disrupting the viral envelope; however, the concentrations that are required for effective inhibition are in the medium-to-high micromolar range, which is likely too high for prophylactic or therapeutic applications.

Design and Synthesis of Optimized Tweezers

To develop advanced tweezers with increased antiviral activity, we introduced a broad variety of anchor groups into both tweezer phosphates. The underlying idea is that additional hydrophobic units protruding from the tweezer body will also be inserted into the viral membrane, increase its rigidity and surface tension, and lead to facilitated disruption. In fact, a preliminary SAR study with nine CLR01 derivatives containing aliphatic ester arms resulted in the identification of advanced tweezers with increased anti-HIV-1 activity.[14] We decided to perform a more systematic SAR study and attached to CLR01 various hydrophobic structural elements as mimetics of integral lipid components found in cell and viral membranes (Figure 2). Simple alkyl tails of varying lengths imitate fatty acids, while double and triple bonds introduce additional elements of increased rigidity. Aromatic moieties offer enlarged π faces for elevated dispersive attraction similar to steroids. All these anchor groups were attached as phosphate monoesters to allow their insertion and parallel alignment within the existing lipid bilayer.

A few chemical reactions allow the selective introduction of exactly one ester group into existing monophosphate esters. In a recent study, we discovered that phosphate activation with trichloroacetonitrile (TCA) indeed allows the introduction of aliphatic primary and small secondary alcohols into the parent tweezer in its diphosphoric acid form (1 in Figure 2a).[19] The scope of the TCA reaction was now greatly expanded, and a total of 34 new two-armed diphosphate esters were prepared in high yields. However, chromatographic purification was necessary at the stage of the phosphoric acid and could not be conducted on the anionic form. Purification was realized by preparative HPLC chromatographic separation over RP-18 silica gel. The resulting phosphoric acid derivatives were quantitatively deprotonated to afford disodium salts with high water solubility. All products displayed very high purity (95–99%) according to HPLC, NMR, and MS.

Figure 2b depicts all new compounds in groups of similar chemical structure and size. Linear and some branched aliphatic alcohols from C1 to C18 were selected to probe for optimal insertion into the lipid bilayer. We tested examples of

https://doi.org/10.1021/jacsau.2c00220
JACS Au XXXX, XXX, XXX−XXX

Table 1. IC_{50}, CC_{50}, and Selectivity Indices (SI) of Tweezers Categorized by Their Chemical Structures[a]

#	tweezer	IC_{50} (μM)	CC_{50} (μM)	SI	#	tweezer	IC_{50} (μM)	CC_{50} (μM)	SI
1	CLR01	35.5	>300	>8.4	20	p-CH204	11.3	177.0	15.6
2	CLR03		>300		21	CP012	15.2	>300	>19.7
3	CLR05	33.0	116.7	3.5	22	CP038	15.3	>300	>19.6
4	PC	49.8	228.0	4.5	23	CP021	16.2	>300	>18.5
5	p-CH200	23.6	213.6	9.0	24	p-CH206	14.9	123.3	8.2
6	p-CH201	29.5	>300	>10.1	25	p-CH192	40.6	243.9	6.0
7	p-CH202	29.2	291.1	9.9	26	p-CH193	15.5	>300	>19.3
8	CP037	15.6	225.6	14.4	27	CP019	1.7	208.0	122.3
9	CP041	37.4	>300	>8.0	28	CP013	14.0	240.0	17.1
10	CP015		295.6		29	CP020	1.0	213.1	213.1
11	p-CH205	14.2	151.5	10.6	30	CP023	16.8	170.9	10.1
12	CP007	16.1	274.3	17.0	31	CP005	1.8	122.3	67.9
13	CP008	24.3	128.2	5.2	32	CP006	2.4	75.9	31.6
14	CP002	2.6	97.0	37.3	33	CP024	1.6	77.4	48.3
15	CP009	8.8	185.3	21.0	34	CP025	6.9	106.1	15.3
16	CP018	6.4	185.4	28.9	35	CP026	1.6	117.9	73.6
17	CP022	6.0	194.3	32.3	36	CP027	1.5	83.8	55.8
18	CP033	29.6	>300	>10.1	37	CP036	2.9	40.8	14.0
19	p-CH203	13.7	184.4	13.4	38	CP049	41.9	292.2	6.9

[a]IC_{50} against SARS-CoV-2 spike-mediated transduction and CC_{50} values in Caco2 cells were calculated by GraphPad Prism from data shown in Figure 3 and Figure S7. The selectivity index (SI) is defined as the quotient of CC_{50} and IC_{50}.

very short length (C1−C3 alkyls such as p-CH200, p-CH201, pCH-202, and CP037), medium length (C4−C5 alkyls such as p-CH205, CP002, CP007, CP008, CP009, CP018, and CP022), extended length (C6−C7 alkyls such as CP013, CP019, CP020, and CP023), and lipid-like length (C8−C18 such as p-CH192, p-CH193, and p-CH206). However, earlier investigations demonstrated that alkyl chains may be included in the hydrophobic tweezer cavity, and interfere with guest binding, exploiting the nonclassical hydrophobic effect and dispersive interactions. We therefore also chose ester alcohols containing terminal triple bonds (C3−C6 alkynes such as p-CH203, p-CH204, CP012, CP021, and CP038). NMR titrations of such tweezer derivatives indicate repulsion of the electron-rich cavity and the π-systems of the ester arms, monitored by the absence of upfield shifts and restored tweezer affinities to cationic guests.[19] Aromatic groups are characterized by their extended flat and rigid π-system and as such undergo extensive interactions inside lipid bilayers.[20] They may be compared with rigid natural lipids such as steroids and are prone to undergo self-assembly inside membranes as artificial lipid rafts.[21] Accordingly, we built a variety of molecular tweezers with two aromatic ester arms (Figure 2b: aromatics). Benzylic alcohols were preferred over phenols with their acidic OH group (pK ∼11), which do not react under the TCA reaction conditions. These included benzene (CP005, CP024, CP025, CP026, and CP027), naphthalene (CP006), and biphenyl (CP036) ring systems. Finally, some charged alcohols were included into the test series, intended to establish additional ionic interactions with the choline or phosphate head groups of most phospholipids (ionic groups such as CP015, CP033, CP041, and CP049).

Properties of the New Tweezers

Since an open tweezer cavity is a prerequisite for the efficient inclusion of a choline head group, several experiments were conducted to elucidate this situation in the series of new tweezer derivatives. Especially, the aliphatic two-armed tweezers experience significant upfield shifts of their hydrophobic ester moieties in aqueous buffer (C1−C3 alkyl, C4−C5 alkyl, C6−C7 alkyl, and C8−C18 alkyl). The chemical shifts of the ester protons correlate directly with their degree of self-inclusion and give hints on the local chemical environment of the ester arms: In general, P−O−CH and P−O−CH_2 protons as well as internal CH_2 and even terminal CH_3 protons experience upfield shifts between 0 and 2 ppm. Interestingly, these never exceed the half-maximal value for complete guest inclusion, known from tweezers with only one self-included alkyl group (∼4 ppm).[19] Since fast exchange leads to averaged NMR signals, we tentatively propose that, for steric treasons only, one ester arm resides inside the cavity, while the other ester group remains outside (Figure S3). The exact nature of the self-inclusion in CP020 could be derived from a polarity shift experiment, with incremental changes from pure DMSO-d_6 to pure D_2O (Figure S4). In the heptyl ester arms, moderate upfield shifts were detected for the $POCH_2$ group as well as the terminal CH_3 protons, while massive upfield shifts of up to 2.5 ppm occurred in the internal C3−C4 methylene groups, indicating that one ester arm is threaded through the tweezer cavity. To visualize the effect of the self-included alkyl arms on the tweezer lipid affinity, we conducted an NMR titration experiment between CP020 (C7 arms) and phosphosphingomyelin SM in methanol where both compounds are soluble and do not aggregate (Figure S5). As expected, a 15 mM affinity was determined, 2-fold weaker than that of the parent tweezer CLR01 (K_D = 8 mM). It should be noted that self-inclusion in free aqueous solution may be overcome when the tweezers approach the membrane and the dielectric constant rapidly decreases. Here, the choline head group inserts into the tweezer cavity and the alkyl arms are free to interact with the lipid bilayer.

By sharp contrast, the electrostatic repulsion of the tweezer π-systems prevents unsaturated aliphatic chains from threading and keeps the cavity open. Indeed, all terminal alkynes (C3−C6 alkynes) show only small upfield shifts of their nonincluded ester arms. Aromatic ester groups with their extended π-system (aromatics) are even better in this respect and do not touch the tweezer cavity.

https://doi.org/10.1021/jacsau.2c00220
JACS Au XXXX, XXX, XXX−XXX

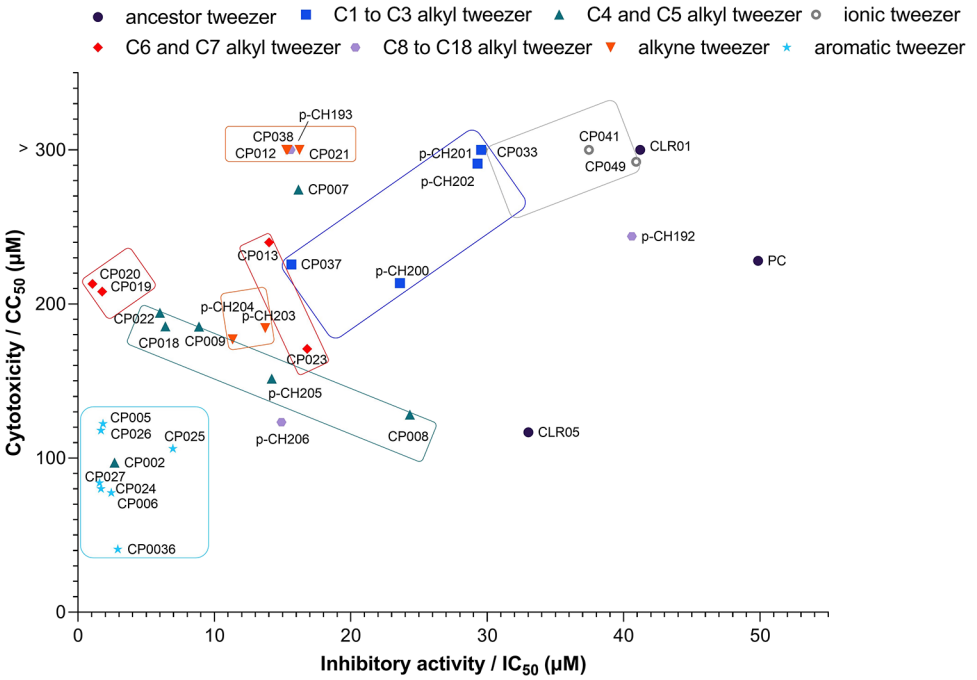

Figure 3. Correlation of antiviral and cytotoxic activities of tweezers. IC_{50} and CC_{50} values shown in Table 1 were plotted against each other, revealing a significant structure-activity relationship because tweezers with similar structure form clusters.

Table 2. Overview of the IC_{50}/EC_{50} Values of Tweezers against Enveloped Viruses and Liposomes[a]

#	tweezer	SARS-CoV-2 IC_{50} (μM)	SI	RSV IC_{50} (μM)	SI	IAV IC_{50} (μM)	SI	MeV IC_{50} (μM)	SI	HIV-1 IC_{50} (μM)	SI	liposome EC_{50} (μM)
1	CLR01	26.5	>11.3	61.5		30.5	>9.8	78.4	>3.8	33.3	>9.0.	79.2
2	CLR03			n.a.	n.a.					n.a.	n.a.	
3	CLR05	n.a.	n.a.	n.a.	n.a.	70.3	1.6	70.4	>4.2	27.1	n.a.	120.8
4	CP002	8.2	11.8	n.a.	n.a.	2.8	34.6	2.8	91	1.1	78.0	4.4
5	CP022	19.9	9.7	n.a.	n.a.	34.5	5.6	13.4	>22.3	4.4	n.a.	19.4
6	CP012	97.4	>3.0	n.a.	n.a.	38.4	>7.8	28.0	>10.7	5.4	n.a.	60.9
7	CP038	48.9	>6.1	18.9	>15.8	192.6	>1.5	30.1	>9.6	6.9	n.a.	43.4
8	CP021	64.9	>4.62	n.a.	n.a.	46.5	>6.4	41.3	n.a.	11.4	n.a.	90.3
9	CP019	1.0	208	7.4	>40.5	112.6	1.8	4.6	>65.2	1.8	104.5	6.5
10	CP013	n.a.	n.a.	n.a.	n.a.	6.7	35.8	5.1	>58.8	2.5	69.4	n.a.
11	CP020	0.4	532.7	7.1	>42.2	24.5	8.6	4.0	>75	1.6	62.9	4.4
12	CP023	2.6	65.7	n.a.	n.a.	16.7	10.2	7.4	>40.5	4.1	35.1	18.0
13	CP005	8.5	14.3	n.a.	n.a.	8.0	15.2	2.7	>111.1	1.9	46.8	4.0
14	CP006	0.3	253	6.0	>50	0.6	126.5	3.0	>100	0.9	82.6	4.8
15	CP024	1.5	51.6	n.a.	n.a.	2.1	36.8	2.1	81.8	1.8	33.6	3.0
16	CP025	0.6	176.8	6.1	27.8	3.2	33.1	7.0	24.2	1.1	40.0	6.9
17	CP026	1.8	65.5	n.a.	n.a.	11.6	10.1	1.9	>157.8	1.5	48.3	2.6
18	CP027	7.0	11.9	n.a.	n.a.	3.8	22.0	1.6	153.3	1.1	63.5	3.7
19	CP036	0.2	204	9.7	19.7	0.6	68.0	8.1	23.5	2.1	13.9	14.1

[a]n.a.: not analyzed.

Effect of New Tweezers against SARS-CoV-2 Spike Pseudoparticle Transduction

We determined the antiviral activity of all synthesized tweezers and controls. Due to the large number of compounds, the high-throughput SARS-CoV-2 spike pseudoparticle system was used. All analyzed new tweezers (with the exception of CP015 that contains a choline head group) suppressed transduction in a concentration-dependent manner (Figure S6), and 30 of 37 tweezers were more potent than the parental CLR01 molecule (IC_{50} of 35 μM) (Table 1). The addition of C1 to C3 alkyl moieties to CLR01 resulted in tweezers with modestly increased antiviral activities (IC_{50} values ranged from 16 μM to 37 μM) (Figure S6a). Alkyne (Figure S6b) and C4/C5 alkyl tweezers (Figure S6c) were on average more active than C1−C3 alkyl derivatives, with p-CH204 (IC_{50} of 11 μM) and CP002 (IC_{50} of 2.6 μM) as most potent representatives. The tweezer with the most potent antiviral activity was CP020, a C7 alkyl derivative, with an IC_{50} of 1.0 μM (Figure S6d). The C6 alkyl derivative CP019 was also very active with an IC_{50} value of 1.7 μM (Figure S6d). The addition of longer C8 to C18 alkyl chains (p-CH192, p-CH193, and p-CH206) did not further increase antiviral activity and resulted in moderately active tweezers with IC_{50} values ranging from 15 to 41 μM (Figure S6e). Most of the aromatic tweezers potently inhibited

https://doi.org/10.1021/jacsau.2c00220
JACS Au XXXX, XXX, XXX−XXX

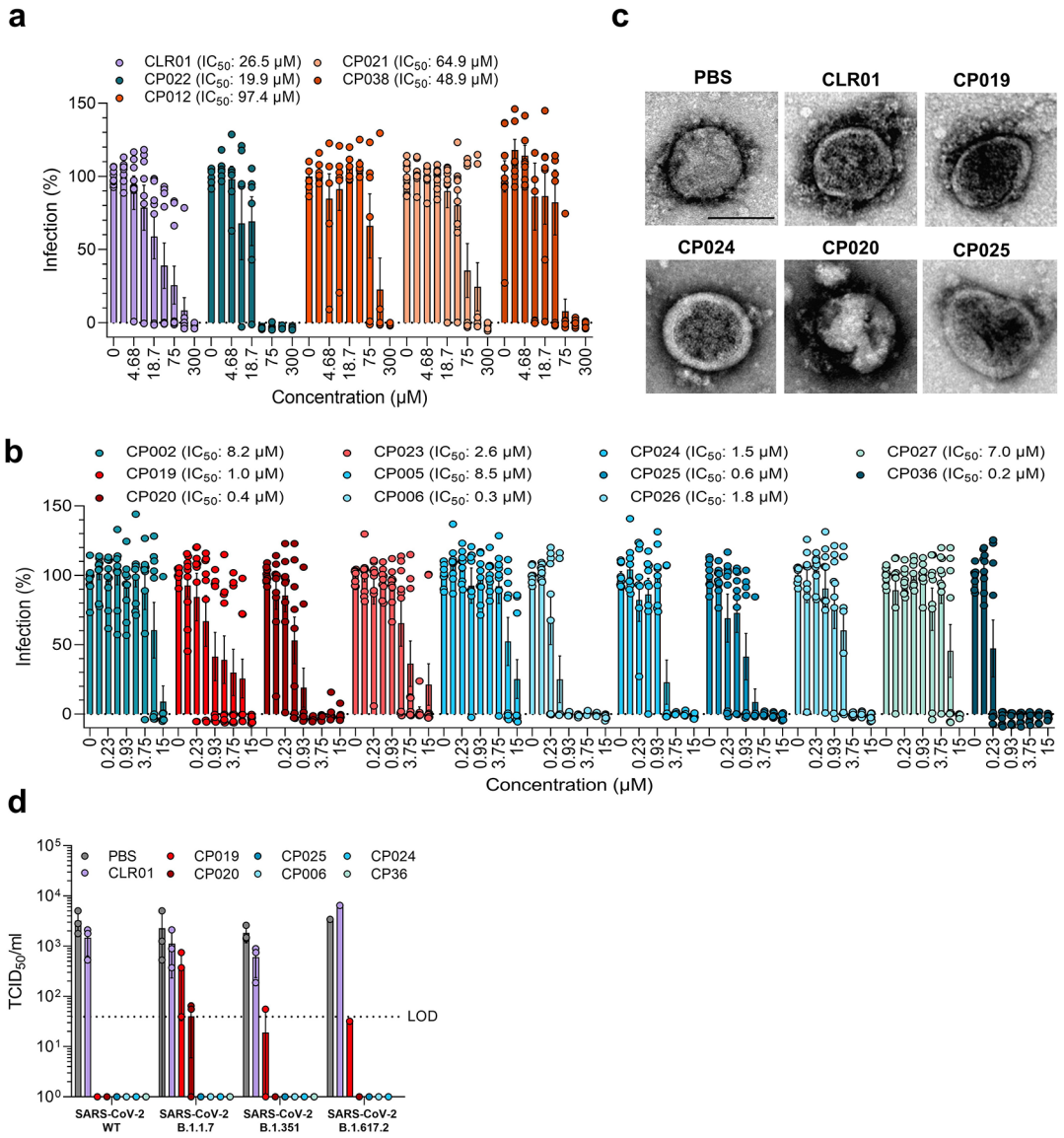

Figure 4. Advanced tweezers inactivate SARS-CoV-2. (a, b) Selected tweezers inhibit SARS-CoV-2 infection. SARS-CoV-2 (MOI 0.0007) was exposed to 2.3−300 μM on virus (a) or 0.1−15 μM on virus (b) of indicated tweezers for 2 h at 37 °C and added to Caco2 cells. Infection rates were determined 2 days later by nucleocapsid specific in-cell ELISA. Values represent infection rates (means) normalized to mock infected controls and were derived from two or three independent experiments each performed in triplicates (±SEM). (c) Tweezers destroy SARS-CoV-2 particles. SARS-CoV-2 was mixed with PBS, CLR01 (250 μM), or advanced tweezers (50 μM), incubated for 30 min at 37 °C, fixed, stained with uranyl acetate, and visualized via TEM. Scale bar = 100 nm. For more TEM images and quantification, see Figure S8. (d) Tweezers inactivate SARS-CoV-2 VOC B.1.1.7 (Alpha), B.1.351 (Beta), and B.1.617.2 (Delta). Virus stocks were mixed with CLR01 and optimized tweezers (50 μM) and incubated for 2 h at 37 °C. $TCID_{50}$ was performed by addition of serial dilutions of the sample on Vero E6 cells. The virus-induced cytopathic effect was determined 5−7 dpi and $TCID_{50}$ calculated according to Reed and Muench.[22] LOD defines as the limit of detection of the method. Values were derived from one (Delta) to three (WT, Alpha, and Beta) independent experiments (±SD).

SARS-CoV-2 spike pseudoparticle transduction, with CP005, CP024, CP026, and C027 as the most active ones (IC_{50} values between 1.5 and 1.8 μM) (Figure S6f). Thus, the structure-activity relationship study allowed us to increase the antiviral activity of CLR01 by more than one order of magnitude.

As modifications of CLR01 may also alter cytotoxic properties, we determined the half-maximal cellular cytotoxicity (CC_{50}) of all tweezers and calculated the respective selectivity index (SI) (Figure S7, Table 1). Because of solubility issues and limited amounts of materials, the highest applied concentration of the tweezers in cell culture was 300 μM. Under these conditions, CLR01 and seven new tweezers (p-CH201, CP041, CP033, CP012, CP038, CP021, and CH193) showed little or no cytotoxicity (CC_{50} > 300 μM). The remaining tweezers affected cell viability to a certain degree, with corresponding SI values between 5 (CP008) and 200 (CP020) (Table 1). Interestingly, graphical representation of antiviral activity and cytotoxicity reveals a structure-activity relationship depending on the side arm moiety of the tweezer (Figure 3). In general, the inhibitory activity improves with the increasing length of simple alkyl chains, from the ancestor tweezer (purple) over C1−C3 (blue) and C4−C5 (green) to C6−C7 (red), while toxicities are low (Figure 3). Further elongation of alkyl chains results in the loss of activity and increased toxicity (light purple). Alkyne tweezers on the contrary are even less toxic than their alkyl counterparts (CC_{50}

https://doi.org/10.1021/jacsau.2c00220
JACS Au XXXX, XXX, XXX−XXX

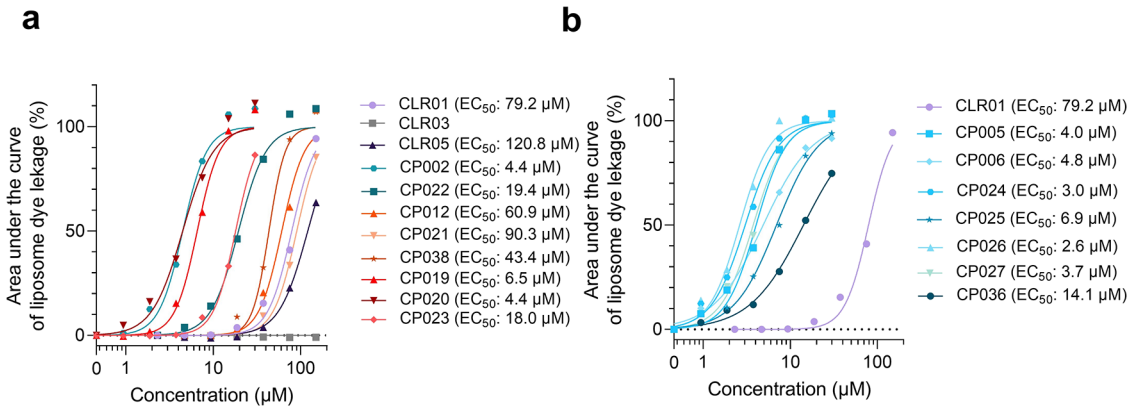

Figure 5. Tweezers disrupt virus-like liposomes. (a, b) 200 nm sized DOPC/SM/Chol (45/25/30 mol %) liposomes filled with 50 mM carboxyfluorescein were incubated with escalating concentrations of alkyl (a) or aromatic (b) tweezers for 30 min after measuring baseline fluorescence for 5 min. Dye leakage was recorded by fluorescence measurement at 485 nm extinction and 528 nm emission. Complete leakage was induced by 1% Triton X-100; values were corrected for baseline and normalized to maximum fluorescence. The graph shows the area under the curve for each tweezer concentration. Values represent means of one experiment performed in triplicate.

> 300 μM) (orange). The most powerful antiviral activity was found for the group of aromatic esters (light blue). Their similarity to rigid steroids seems to be responsible for the highest degree of viral destabilization, most likely by forming lipid rafts. However, this goes at the cost of cytotoxicity (CC_{50} around 100 μM). The ionic sidechains provide no improved inhibition (gray), indicating that, for efficient anchoring, a deep insertion into the hydrophobic membrane interior is a prerequisite (Figure 3 and Table 1). Taken together, we identified two lead structures: first, C6 (CP019) and C7 (CP20) alkyl arms (red area in Figure 3) provide high antiviral efficacy and minimal toxicity; and second, tweezers with aromatic arms (CP005, CP006, and CP025−CP027), which are even more potent antivirals but show some cytotoxicity (light blue area in Figure 3).

Advanced Tweezers Inactivate SARS-CoV-2

Based on the antiviral activity against spike pseudoparticles (low IC_{50} values), high SI, ease of chemical synthesis, and structural differences, we selected 15 novel tweezers for further characterization (Table 2) and determined their activity against live SARS-CoV-2. Tweezers CP038, CP022, CP021 (Figure 4a), and CP002 (Figure 4b) inhibited viral infection with IC_{50} values comparable to CLR01, with a median IC_{50} of 27 μM (Table 2). CP012 was least active (IC_{50} of 97 μM). All other tested tweezers suppressed SARS-CoV-2 infection with IC_{50} values below 10 μM (Figure 4b, Table 2). Aromatic tweezers CP036 (IC_{50} of 0.2 μM), CP006 (IC_{50} of 0.3 μM), and CP025 (IC_{50} of 0.6 μM) as well as the C7 alkyl tweezer CP020 (IC_{50} of 0.4 μM) were the most potent compounds with activities in the nanomolar range (Figure 4b).

To visualize the effect of tweezers on the SARS-CoV-2 morphology, we again performed TEM. Note that the detection of virions by TEM requires a high concentration of viral particles and consequently a high concentration of tweezers for inactivation (Figure S1d). In the presence of tweezers, virions appeared damaged, which can be seen by distortion of their spherical morphology, notches in the envelope, and, in most cases, an electron-dense virion center, indicating disruption of the viral membrane upon tweezer treatment (Figure 4c and Figure S8). In agreement, pretreatment of cells with antivirally active concentrations of CLR01 or selected optimized tweezers, followed by subsequent inoculation with virus, did not affect viral infectivity (Figure S9), confirming that the antiviral activity of tweezers is directed against the virus. Finally, we analyzed whether advanced tweezers may also inactivate SARS-CoV-2 variants of concern (VOCs) B.1.1.7 (Alpha), B.1.351 (Beta), and B.1.617.2 (Delta). As shown by $TCID_{50}$ analyses, 50 μM advanced tweezers inactivated all the SARS-CoV-2 variants (Figure 4d), suggesting that the tweezers have broad anti-SARS-CoV-2 activity and may also inactivate other upcoming VOCs.

Tweezers Retain Antiviral Activity in the Presence of Airway Mucus

CLR01 loses antiviral activity in the presence of human serum, which prevents its systemic administration as an antiviral drug.[13] Thus, the preferred mode of application of tweezers is topical, either on anogenital surfaces as a prophylactic or therapeutic agent against sexually transmitted pathogens or on mucosal surfaces of the respiratory tract to protect from or prevent dissemination of respiratory viruses. Thus, we analyzed whether CLR01 and advanced tweezers are antivirally active in the presence of mucus, which covers and protects epithelial cells of the respiratory tract. Mucus (including airway surface liquid) was collected from human airway epithelial cells (from two donors) grown at the air−liquid interface as previously described[23] and mixed with SARS-CoV-2 spike pseudoparticles. Samples were then treated with CLR01 or the advanced tweezers CP019 and CP020 and used to transduce Caco2 cells. As shown in Figure S10, mucus did not affect the antiviral activity of the analyzed tweezers.

Advanced Tweezers Disrupt Virus-like Vesicles

We have previously shown that the antiviral activity of tweezers against HIV-1 correlates with their ability to disrupt liposomes formed by a virus-like lipid bilayer consisting of 1,2-dioleoyl-*sn*-glycero-3-phosphocholine (DOPC), sphingomyelin (SM), and cholesterol (Chol), with a ratio of 45/25/30 mol %.[14] Here, we studied liposomal membrane disruption in a liposome dye leakage assay and found that all antivirally active tweezers achieved a concentration-dependent disruption of the liposomal membrane (Figure 5, Table 2). Except for the inactive control tweezer derivative CLR03, CLR05 (Figure 5a), and CP036 (Figure 5b), all tweezers induced complete leakage. CP002, CP019, and CP020 were the most potent alkyl tweezers with half-maximal effective concentrations (EC_{50}) of

https://doi.org/10.1021/jacsau.2c00220
JACS Au XXXX, XXX, XXX−XXX

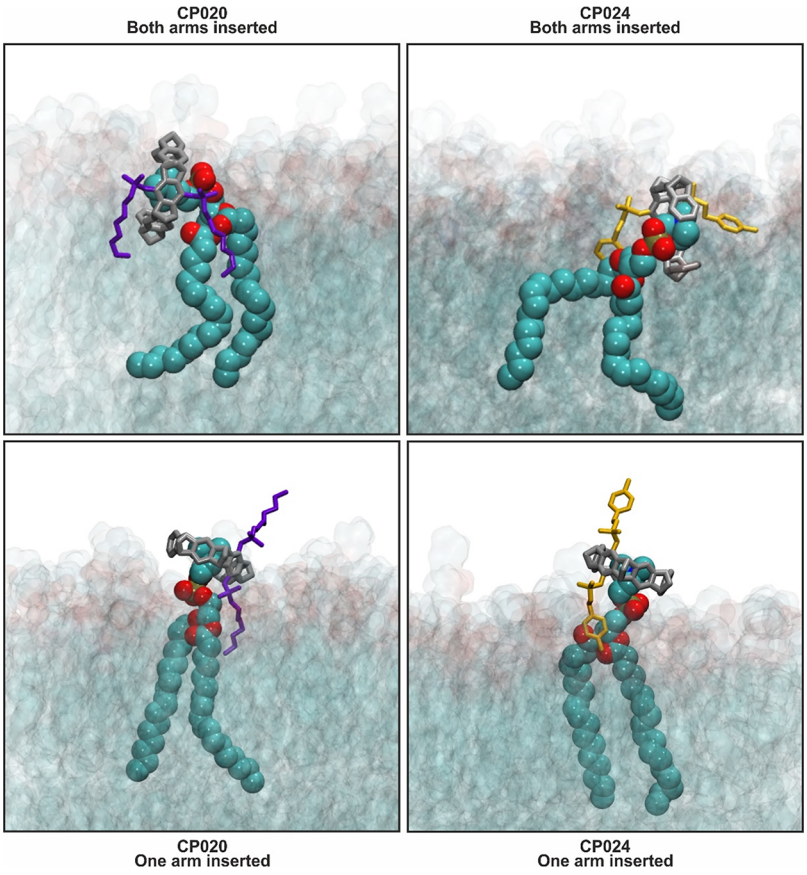

Figure 6. Advanced molecular tweezers can incorporate their side arms into the lipid membrane. CP020 arms are represented in violet, and CP024 arms are shown in yellow. The core of the tweezers is shown in gray. The membrane is rendered transparent to allow the visualization of the inserted arms. The lipid complexed with the tweezer is highlighted with van der Waals representation. Water molecules and the hydrogen atoms of the tweezers and of the bound lipids are omitted for clarity.

4.4, 6.5, and 4.4 μM (Figure 5a). Most aromatic tweezers induced dye leakage with EC_{50} values in the one-digit micromolar range, with CP024 (EC_{50} of 3 μM) and CP026 (EC_{50} of 2.6 μM) as most potent compounds (Figure 5b, Table 2). Correlation analysis of liposomes and SARS-CoV-2 spike pseudoparticles reveals significant similarity, thus further corroborating that viral membrane disruption underlies the antiviral activity (Table S4, Figure S11).

Advanced Tweezers Incorporate Their Side Arms into the Lipid Membrane

To investigate the mechanism of disruption of viral membranes by the potentiated tweezers, we performed extensive Gaussian accelerated Molecular Dynamics simulations (GaMD). The membrane, simulated using a similar setup (see the Supporting Information) as in our previous study with the CLR01 tweezer,[14] was composed of DOPC, SM, and Chol in a 54:30:36 ratio, for a total of 120 lipids molecules on each leaflet of the membrane. The C7 alkyl tweezer CP020 and the aromatic tweezer CP024 were chosen for extended simulations as promising candidates from the experimental results. The simulations showed that, similar to CLR01, both CP024 and CP020 bind to the lipid's head by incorporating its cationic ammonium into the tweezers' cavity. Several binding events were observed in all replicas of the simulations (Figure S12a, Tables S1, S2, and S3), and the tweezers–lipid complexes were conserved (in one case, the complex was briefly lost only to be formed again). Similar to CLR01, none of the tweezer units crossed the membrane during the whole sampling in any replica of the simulations. In addition, we performed GaMD simulations (see Biomolecular Modeling for details) with CP026 since together with CP024, this tweezer was found to be very effective in the liposome dye leakage assay. The simulations indicated a similar behavior of CP026 with respect to CP024 (Figure S13).

We previously reported that binding of CLR01 effectively changes the orientation of the lipid's head group by nearly 90° with respect to its normal orientation in the membrane. By doing so, the tweezer destabilizes the membrane.[14] Here, we analyzed the distribution of the tilt angles of the unbound lipids (from the lower leaflet) in the membrane and compared it to those of the membrane lipids bound to tweezers from the upper leaflet. We used CP024 for this purpose (Figure S12b). Our study reveals a predominant tilt angle at around 60–80° for unbound lipids. Interestingly, the tilt angles of tweezer-bound lipids shift to 80–110°, a similar effect to what was observed for CLR01 (Figure S12b). Additionally, the simulations show that CP020 and CP024 are able to introduce their functionalized arms into the membrane (Figure 6). This effect will increase the steric congestion and stiffness of the surrounding lipid raft and consequently increase surface tension. We also observed during the simulations the formation of tweezer–tweezer complexes due to the interaction of the cavity of one tweezer with the hydrophobic core of another tweezer. The presence of elongated arms in these tweezers also allows forming inclusion complexes with

https://doi.org/10.1021/jacsau.2c00220
JACS Au XXXX, XXX, XXX–XXX

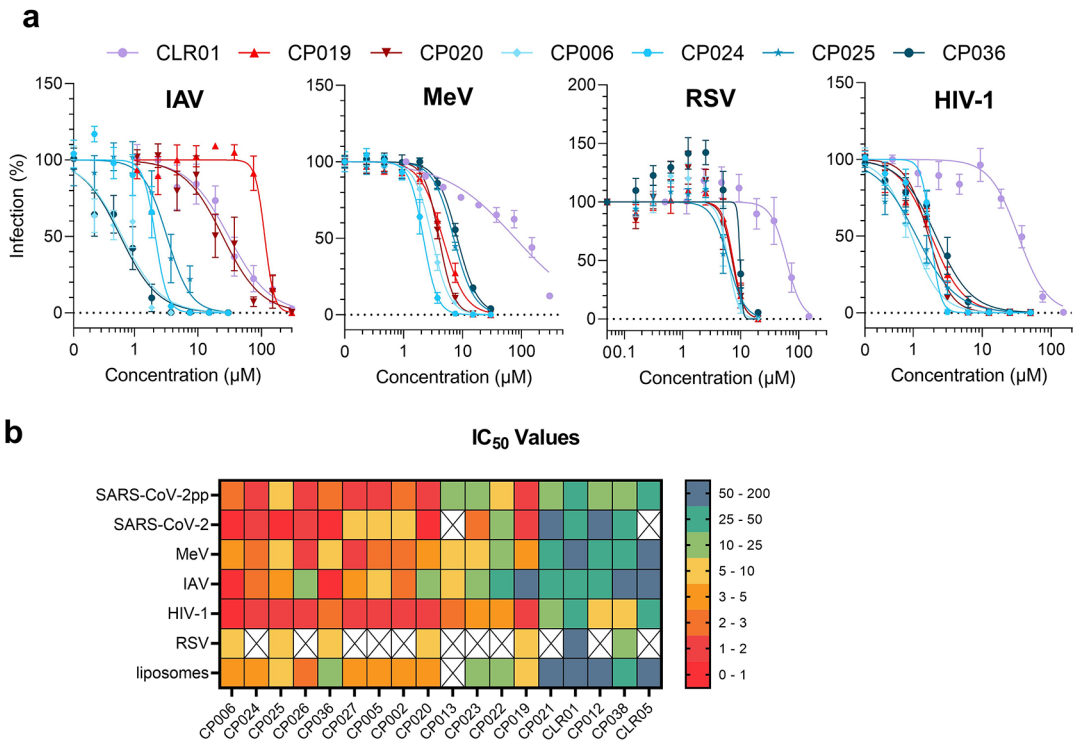

Figure 7. Antiviral activity of advanced tweezers against enveloped respiratory pathogens and HIV-1. (a) IAV was incubated with tweezers for 30 min at 37 °C before adding to Caco2 cells. Two days later, viral neuraminidase activity was quantified in cellular lysates by the MUNANA assay. MeV encoding GFP was incubated with tweezers for 30 min at 37 °C before adding to A549 cells. Two days later, infection was quantified using flow cytometry analysis. RSV encoding GFP was incubated with tweezers for 30 min and used to inoculate A549 cells. One day later, infection was quantified by flow cytometry. HIV-1 was incubated with tweezers for 10 min at 37 °C before adding to TZM-bl reporter cells. Infection rates were determined 3 days later by quantifying β-galactosidase activity in cellular lysates. Values represent mean infection rates normalized to mock infected controls and are derived from two (in the case of MeV) or three independent experiments each performed in triplicate (±SEM). (b) Heat map showing IC_{50} and EC_{50} values of tweezers against viruses and liposome.

other tweezers units instead of the lipid's head. We observed during the simulations that the arm of one tweezer can insert into the cavity of another and form a dimer (Figure S14). Tweezer−tweezer complexes preclude the formation of inclusion complexes with the head of the lipids and result in tweezers agglomerates in the solvent phase, as observed during the simulations. However, these interactions are weaker compared to the lipid−tweezers interactions since the hydrocarbon core and functionalized arms of CP020 and CP024 are not positively charged, unlike the lipid's head group.

Advanced Tweezers Are Broad-Spectrum Inhibitors of Enveloped Viruses

We evaluated the antiviral activity of the tweezers against other respiratory pathogens. For this, IAV, MeV, and RSV were treated with escalating concentrations of tweezers and then used to inoculate respective target cells. As tweezers are currently developed as microbicides, we also included a sexually transmitted pathogen, HIV-1. IAV infection rates were determined by quantifying intracellular neuraminidase activity by a MUNANA assay, MeV and RSV infection were quantified by flow cytometry detection of GFP expressing cells and HIV-1 infection by a TZM-bl reporter assay (Figure 7a, Figure S15). All tweezers inhibited IAV, MeV, RSV, and HIV-1 infection in a concentration-dependent manner, without showing toxicity at the used concentrations (Figures S7, S16, and S17). IC_{50} values of the most potent tweezers are in low micromolar and high nanomolar ranges (Table 2). Generally, C6/C7 alkyl and aromatic tweezers showed a better pan-antiviral activity and high SI values as compared to the other variants (Figure 7b, Table 2). The antiviral activity against MeV, RSV, and HIV-1 correlated well among each other, with those obtained with lentiviral SARS-CoV-2 spike pseudoparticles and with the potency to lyse virus-like liposomes (Table S4, Figure S11). Notably, no correlation was observed for antiviral activity against IAV or SARS-CoV-2 with those of other viruses or liposomes (Table S4).

Antiviral Activity of Tweezer against RSV and SARS-CoV-2 in Mice

Having demonstrated that tweezers exert broad antiviral activity in cell culture, we next evaluated the effect of the selected tweezers on RSV infection of mice. For this, we exposed RSV to 2 mM of CLR01, inactive CLR03, or buffer in a volume of 50 μL and immediately infected BALB/cJ mice via the intranasal route. At day 5 post infection, mice were sacrificed, and lungs were collected, homogenized, and subjected for viral RNA load analysis by RT-qPCR. As shown in Figure S18, CLR01, but not CLR03, completely abolished RSV infection. We then moved on and tested the effect of the advanced tweezers CP006, CP019, and CP025 on SARS-CoV-2 infection of K18-hACE2 mice (n = 6 per group), using a similar maximum efficacy setting. In brief, SARS-CoV-2 was exposed to buffer control (PBS) or tweezers (150 μM), and then mixtures were applied after 1 min incubation via the intranasal route. Seven hours later, mice received a second treatment with PBS or tweezers. Mice were monitored for

https://doi.org/10.1021/jacsau.2c00220
JACS Au XXXX, XXX, XXX−XXX

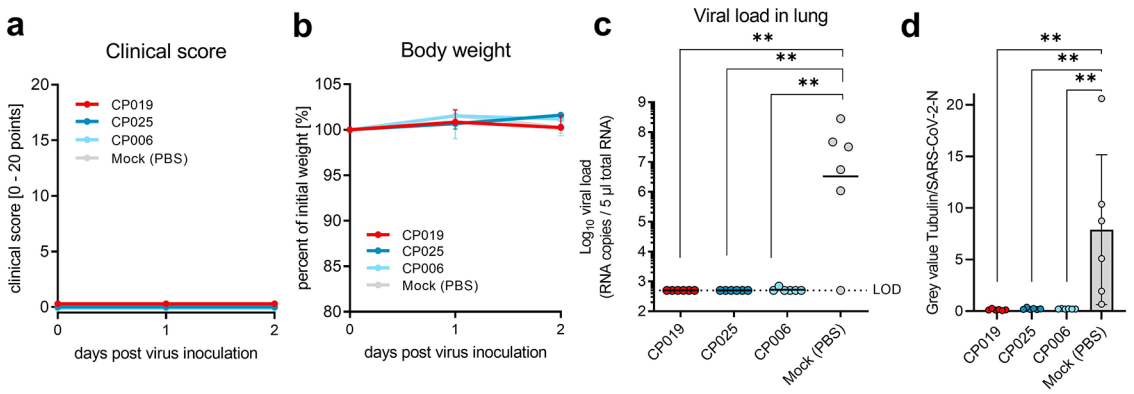

Figure 8. Molecular tweezers reduce viral load in the lungs of SARS-CoV-2-infected mice. (a, b) Tweezers (150 μM) or PBS were mixed with SARS-CoV-2, and after 1 min incubation, the mixture was applied via an intranasal route in 50 μL total volume into transgenic K18-hACE2 mice (n = 6). Seven hours after infection, the mice received a second treatment at the same doses. Mice were monitored daily for the body weight and clinical score. (c) On day 2 post-infection, mice were sacrificed and their lungs were collected, homogenized, and subjected for viral RNA load analysis by RT-qPCR. Viral loads are shown for each individual mouse in addition to the geometric means of each group. Statistical analysis was done using one-way analysis of variance (ANOVA) with the Kruskal–Wallis test and Dunn's Pairwise Multiple Comparison Procedures as *post hoc* test (** = $p < 0.01$). (d) Western blot analysis of SARS-CoV-2 Nucleocapsid and Tubulin expression in mice lung homogenates of (c). Intensity of bands was quantified by Fiji's (ImageJ) built-in gel analysis tool (see Figure S19 for the gel image). Statistical analysis was done using ordinary one-way ANOVA with Dunn's Pairwise Multiple Comparison Procedures (** = $p < 0.01$).

body weights and clinical scores for 2 days, but no significant side effects were observed (Figure 8a,b). At the end of day 2, mice were euthanized, and lungs were collected, homogenized, subjected to viral RT-qPCR (Figure 8c), and to Western blot analysis for the viral N protein (Figure 8d and Figure S19). Viral RNA and N-protein expression could be quantified in 5 out of 6 mice in the control group (3.27×10^6 to 5.0×10^2 for CP019 and CP025 and 5.28×10^2 for CP006 copies/mL in lung homogenate) showing productive SARS-CoV-2 infection of the lungs. In contrast, tweezer treatment completely abolished SARS-CoV-2 infection of all tested mice (Figure 8c,d, Figure S19).

DISCUSSION

We present here a series of novel advanced molecular tweezers with broad-spectrum antiviral activity against enveloped viruses. Lead compounds such as CP020, CP025, CP019, and CP036 inhibit viral infectivity *in vitro* at sub-micromolar concentrations and exhibit high selectivity indices suggesting a favorable therapeutic window for topical applications. Furthermore, the maximum efficacy study in mice demonstrated that treatment of RSV and SARS-CoV-2 with molecular tweezers effectively abrogated viral infection in the absence of any unwanted obvious side effects.

Molecular tweezers act by a unique mode of action: the phosphate tweezer CLR01 and also the carboxylate tweezer CLR05 bind to lipid heads, in particular to sphingomyelin, which is enriched in the viral membrane.[14,24] Binding allows the tweezers to interact with the membrane leading to high surface tension and membrane disruption. Consequently, CLR01 and CLR05 inactivate HIV-1, IAV, HSV-1, HSV-2, and ZIKV.[12,13] In the present study, we could additionally show that SARS-CoV-2 and other respiratory viruses are inhibited by CLR01. Furthermore, we designed, synthesized, and tested over 34 new tweezers to improve antiviral activity and to achieve high SI values. The performed structure-activity relationship study resulted in potentiated tweezers with activities in the nanomolar range. Addition of hexyl or heptyl ester arms onto CLR01 was most beneficial because it increased antiviral activity with low toxicity. Thus, CP019 and CP020 reached superior SI values of ~208 and ~313, suggesting a large therapeutic window for medical applications. The most powerful introduced side arms, however, were the aromatic groups, albeit at the cost of slightly elevated toxicities with CC_{50} values around 100 μM. With IC_{50} values in the nanomolar range, again high SI values were reached. The improved antiviral activity of all aromatic and hexyl/heptyl tweezers was confirmed for the SARS-CoV-2 variants of concern Alpha, Beta, and Delta.

Tweezers with C6-C7 alkyl arms exhibit the most potent antiviral activity among alkyl tweezers. We tentatively explain this effect with an optimal alkyl length for entering the membrane: short alkyl side arms display too low penetration, while longer alkyl chains might induce permanent self-inclusion and or steric hindrance. Aromatic moieties provide increased rigidity as well as their resemblance of cholesterol might favor membrane insertion and thus increase surface tension.

Simulations revealed that the tweezers may locally increase the surface tension of the membrane by forcing the heads of the lipids to adopt a conformation with larger tilt angles (80 to 110°) than unbound lipids. This destabilizing effect, although local, can be important especially considering the multiple binding events on different regions of the membrane observed during the simulations. Unlike CLR01, the destabilizing effects of CP024, CP026, and CP020 on the modeled viral membranes go beyond the influence on the tilt angle. As observed during the GaMD simulations with CP020, CP026, and CP024, the new tweezers can incorporate their arms into the membrane. This might lead to further increased surface tension and disruption of the membrane around the tweezer–lipid complex. This effect showcases how the rational design of molecular tweezers can enhance their destabilizing effects on the viral membrane.

Our SAR study revealed that tweezer's IC_{50} values obtained for HIV-1, RSV, MeV, and pseudoviruses correlated well with EC_{50} values observed in the liposome leakage assays. HIV-1, RSV, and MeV as well as lentiviral vectors (used for pseudovirus generation) bud through lipid rafts from the plasma membrane and are enriched in cholesterol and

https://doi.org/10.1021/jacsau.2c00220
JACS Au XXXX, XXX, XXX–XXX

sphingomyelin.[24] The liposomes used in this study mimic this lipid composition, explaining the observed correlations. However, no correlation was observed for antiviral activities against SARS-CoV-2 and IAV. Interestingly, SARS-CoV-2 buds from the ERGIC (endoplasmic reticulum−Golgi intermediate compartment) and is thus surrounded by a different lipid envelope than viruses budding from the plasma membrane.[25] Thus, it would be interesting to determine how tweezers disrupt liposomes with SARS-CoV-2-like lipid composition. The lack of correlation for IAV, which also buds from the plasma membrane, remains unclear. It might also be possible that tweezers may interact with lysine and arginine residues[26] in viral glycoproteins, such as the SARS-CoV-2 spike, thereby interfering with the glycoprotein function and infection. Although we cannot rule this out, the main target of the tweezers is most likely the viral membrane, as it has been shown that tweezers also destroy lentiviral particles lacking viral glycoproteins,[12] and that the antiviral activity of the tweezers correlates with the activity in the liposome leakage assay, which is performed in the absence of glycoproteins.

From the perspective of medical applications, we note that tweezers rapidly lose antiviral activity in plasma due to albumin binding[13] but remain antivirally active in human mucus. Thus, after successfully passing preclinical safety studies in animal models and humans, we propose to apply potentiated tweezers as sprays (nasal, mouth, or inhalation) to fight respiratory viral pathogens, in particular SARS-CoV-2, against which prophylactic or therapeutic interventions are most urgently needed. Exemplary, several breakthroughs of SARS-CoV-2 infections despite vaccination have been reported.[27,28] This often leads to mild or asymptomatic infections, however increasing the risk for people, which are not able to get vaccinated or in the case of nonantibody responders.[29] Furthermore, the highly transmissible variants of concern B.1.617.2 (Delta) and B.1.1.529 (Omicron) reduce the effectiveness of vaccines in virus shedding.[7,30,31] Molecular tweezers might be used to reduce spread and viral load as supporting antiviral agents.

Finally, it is important to mention that the next threat of new viral infections of unknown origin can be expected in the near future. As powerful destabilizers for viral membranes, our tweezers provide a generally applicable antiviral principle that can be rapidly implemented for medical intervention.

MATERIAL AND METHODS

Chemicals, Purification, and Characterization of Dialkyl Diphosphate Tweezers

All chemicals in this work were purchased from Sigma-Aldrich, Fisher Chemicals, VWR, Fluka, Acros Organics, and TCI in commercial grade. Tweezer compounds were purified by preparative reversed-phase high-performance liquid chromatography (HPLC) using a Prominence UFLC system of Shimadzu equipped with the reverse-phase column Luna 5 μm C18 (2), 100 × 21.20 mm from Phenomenex. The separation was achieved via a gradient run with acetonitrile/water + 0.1% TFA at a flow rate of 25 mL min^{-1} with peak detection at 210 nm. The Q-TOF mass spectrometer Bruker maXis 4G was used for recording high-resolution electron spray ionization (ESI) mass spectra. For the analysis, 1 μM tweezer solutions were prepared in methanol.^{1}H, ^{13}C, and ^{31}P NMR spectra were recorded with the Bruker AVNeo400 (^{1}H = 400 MHz; ^{13}C = 101 MHz, and ^{31}P = 162 MHz) at 25 °C for every tweezer compound synthesized in this work. NMR titrations were carried out on the Bruker DRX 500 (^{1}H = 600 MHz) at 25 °C.

NMR Titration

^{1}H NMR titration was performed to quantify the interaction between CP020 (host) and phosphosphingomyelin (SM, guest) by monitoring chemical shift changes in the choline head group and deriving the binding constant by nonlinear regression. For this experiment, SM was dissolved in deuterated methanol CD_3OD at c = 0.33 mM. An NMR tube was filled with 600 μL of this lipid guest solution, and the first ^{1}H NMR spectrum was measured. The host solution (c = 10.2 mM) was prepared using the SM solution to keep the guest at a constant concentration, while the host concentration was varied during the titration. The host solution was added in increasing amounts (10−60 μL) leading to effective host concentrations of 0.17, 0.33, 0.49, 0.64, 0.93, 1.20, 1.46, 1.93, 2.35, 2.92, and 3.40 mM. The final host/guest ratio was 10:1. After each addition, the resulting ^{1}H NMR spectra were recorded and chemical shift changes of the $N(Me)_3$, the $P-O-CH_2-CH_2$ and $P-O-CH_2-CH_2$ protons of the choline head group were determined. Eventually, the constants K_A/K_D and the $\Delta\delta_{max}$ values were obtained by nonlinear regression from the resulting binding isotherms.

Polarity Shift Experiment

A second NMR experiment was carried out to characterize the relative content of cavity inclusion of the heptyl side arms of CP020. To this end, the polarity of the solvent was systematically varied by employing different solvent ratios between DMSO-d_6 and D_2O. In this experiment, the first two ^{1}H NMR spectra were measured after dissolving CP020 separately in 600 μL of DMSO-d_6 (tube A) and 600 μL of D_2O (tube B) (each 2 mg, 2.1 μmol, c = 3.4 mM). Subsequently, increasing amounts of deuterated water was added to tube A and increasing amounts of DMSO-d_6 was added to tube B. This resulted in DMSO-d_6:D_2O ratios of 10:0, 9:1, 8:2, 7:3, 6:4, 5:5, 4:6, 3:7, 2:8, 1:9, and 0:10. ^{1}H NMR spectra were recorded after each addition, and the resulting upfield shifts with increasing solvent polarity were monitored for the CH_2 and CH_3 protons of the heptyl chain.

LV(Luc)-CoV-2 Inhibition Assay

To test activity of molecular tweezers against lentiviral SARS-CoV-2 (LV(Luc)-CoV-2) pseudoparticles, tweezers and pseudoparticles were incubated for 30 min at 37 °C with serial dilution of tweezers and subsequently used to transduce Caco2 cells. Transduction rates were assessed after 48 h by measuring firefly luciferase activity using Firefly luciferase assay kit from Promega. To this end, the supernatant was removed, and cells were washed once with PBS and lysed with 40 μL lysis-buffer per well. An amount of 30 μL of these lysates was transferred to a 96-well Nunclon-delta white microwell plate and mixed with 50 μL of luciferase assay substrate. Values represent luciferase activities (measured in relative light units per second, RLU/s) derived from triplicate transductions and normalized to values obtained from transduced cells in the absence of tweezers.

SARS-CoV-2 Inhibition Assay

An amount of 25,000 Caco2 cells was seeded in a 100 μL medium in a 96-well plate. The next day, 44 μL of medium were added on cells. Afterward, 60 μL serial dilutions of tweezers were mixed with 60 μL of SARS-CoV-2 isolate BetaCoV/France/IDF0372/2020 for 2 h at 37 °C. An amount of 36 μL of the tweezer-virus mix was then added on cells, resulting in a multiplicity of infection (MOI) of 0.01 or 0.007. Infection rates were assessed at 2 days post infection by in-cell ELISA for SARS-CoV-2 nucleocapsid or spike.[5] Briefly, cells were fixed by adding 180 μL 8% paraformaldehyde (PFA) for 30 min at room temperature (RT) and permeabilized by incubation with 100 μL of 0.1% TritonX-100 for 5 min. After washing once with PBS, cells were stained with 1:5000 diluted antispike protein antibody 1A9 (Biozol GTX-GTX632604) or an antinucleocapsid antibody (Sinobiological 40,143-MM05) in antibody buffer (10% FCS and 0.3% Tween 20 in PBS) for 1 h at 37 °C. After 2 washes with 0.3% Tween 20 in PBS, the secondary HRP-conjugated antibody (Thermo Fisher #A16066) (1:15,000) was incubated for 1 h at 37 °C. Following three times of washing with 0.3% Tween 20 in PBS, the TMB peroxidase substrate (Medac #52-00-04) was added for 5 min and the reaction

https://doi.org/10.1021/jacsau.2c00220
JACS Au XXXX, XXX, XXX−XXX

stopped using 0.5 M H_2SO_4. The optical density (OD) was recorded at 450 nm with a 620 nm background correction, using the Asys Expert 96 UV microplate reader (Biochrom). Signal derived from uninfected cells was subtracted and untreated controls were set to 100% infection.

SARS-CoV-2 $TCID_{50}$ Endpoint Titration

The infectivity remaining after tweezer virus inhibition was determined by tissue culture infectious dose 50 ($TCID_{50}$). Briefly, tweezer virus mixtures were incubated for 2 h at 37 °C and serially diluted 2-fold followed by inoculation of Vero E6 cells. To this end, 20,000 Vero E6 were seeded per well in 96 flat-bottom well plates in 100 μL medium and incubated over night before 62 μL fresh medium was added. Next, 18 μL of titrated sample was used for inoculation, resulting in final dilutions of $1:10^1$ to $1:10^9$ on the cells in triplicates. Cells were then incubated for 5 to 7 days and monitored for CPE. $TCID_{50}$/mL was calculated according to Reed and Muench.[22]

Negative Staining of SARS-CoV-2 and Electron Microscopy

SARS-CoV-2 isolate BetaCoV/France/IDF0372/2020, produced in a serum-free medium, was mixed 1:1 with respective concentrations of tweezers and incubated for 30 min at 37 °C. Afterward, samples were inactivated by incubation with PFA (2% final concentration) for 30 min at 37 °C and 30 min at RT.[7] Negative-staining transmission electron microscopy was performed according to Laue et al.[8] In brief, 10 μL of the virus supernatants were placed directly onto freshly glow-discharged 300 mesh copper grids, which were coated with a carbon reinforced formvar film. After 10 min adsorption at RT, grids were washed three times with double-distilled water and negatively stained with 0.5% uranyl acetate in water. Virions were imaged with a JEOL JEM-1400 transmission electron microscope operated at 120 kV and quantified. To understand whether the dark stain in the center of damaged virions originated from accumulation of heavy metal stain in an indentation of the virion envelope surface or from a damaged virus envelope and penetration of stain into the virion, tomography was conducted on a JEOL JEM-2100F 200KV microscope in a scanning transmission mode. The sample containing damaged virions was tilted from −50° to 10° in 1.5° increments and the bright-field signal was recorded. Tilt series images were reconstructed to a tomogram with the IMOD software package.[9]

HIV-1 Inhibition Assay

To determine the inhibition rate of HIV-1 by tweezers, HIV-1 NL4-3_92TH014-12 (R5) was incubated 1:1 for 10 min at 37 °C with serial dilution of tweezers, followed by infection of TZM-bl cells in 96-well plate. Infection rates were assessed after 48 h by detecting β-galactosidase activity in cellular lysates using the Tropix Gal-Screen kit (Applied Biosystems) and the Orion microplate luminometer (Berthold) for measurement. Values represent β-galactosidase activities (relative light units per second; RLU/s) derived from triplicate infections and normalized to values obtained for infected cells in absence of tweezer.

MeV Inhibition Assay

To determine the antiviral effect of molecular tweezers, MeV was incubated 1:1 with tweezers in the absence of FCS for 30 min at 37 °C in the respective concentrations. Meanwhile, A549 cells seeded the day before at a density of 20,000 cells per well in a 96-well plate were washed once with PBS before infected with the tweezer/virus mixture reaching a MOI of 0.1 in a volume of 40 μL per well. After 1 h of incubation at 37 °C, 160 μL of respective medium was added and incubated for further 48 h. Infected cells were then washed once with PBS and harvested using 50 μL trypsin per well for 3−5 min until cells were detached. Reaction was stopped with an equal amount of respective medium, and cells were transferred into a 96-V-well plate. After washing cells again, they were fixed in 2% PFA and GFP positive cells were quantified by flow cytometry (CytoFLEX LX, Beckmann Coulter). Data was analyzed by subtracting the background of uninfected cells and normalization to infected cells in the absence of tweezers.

RSV Inhibition Assay

A549 cells were seeded in 48-well plates (2.5×10^4 cells/well) the day before infection. Tweezers at indicated concentrations were incubated with RSV for 30 min at 37 °C prior to infection using MOI of 1 of the pretreated virus. The proportion infected live cells were determined 24 h post infection using flow cytometry by detaching the cells using Trypsin−EDTA prior to staining of the dead cells with a LIVE/DEAD Fixable near-IR Dead Cell Stain Kit (Life Technologies). The data was obtained using a FACSVerse Flow cytometer (BD Biosciences), and the analysis was performed using the FlowJo software (Tree Star).

IAV Inhibition Assay

For inhibition assays, dilutions of tweezers in the serum-free Caco2 medium were mixed with IAV. After 30 min incubation at 37 °C, the mixture was used to infect 40,000 Caco2 cells (MOI 0.0007), which were cultivated in 100 μL cDMEM. After 48 h, infectivity rates were determined by measuring neuraminidase activity in cellular lysates (MUNANA assay). To this end, cells were washed once and lysed for 30 min in 1% TritonX-100. The lysates were diluted 1:2 in MES buffer (containing 32.5 mM MES monohydrate and 4 mM CaCl2 dihydrate). A volume of 20 μL of each sample was transferred to black 96-well plates, and 30 μL 100 μM MUNANA (4-methylumbelliferyl)-*N*-acetylneuraminic acid) were added. After 4 h of incubation at 37 °C and gentle shaking, the reaction was stopped with 150 μL stop solution containing 0.1 M glycine and 25% ethanol. The neuraminidase-dependent cleavage of the substrate to the fluorescent product methylumbelliferone was quantified at an excitation of 360 nm and an emission at 455 nm and was measured on a SynergyTM H1 (BioTek, USA). The background from uninfected cells was subtracted, and relative enzyme activity was used to quantify infection rates.

Biomolecular Modeling

The model bilayer was composed of 54, 30, and 36 molecules of 1,2-dioleoyl-*sn*-glycero-3-phosphocholine (DOPC), sphingomyelin (SM), and cholesterol (Chol), respectively. CP020 or CP024 tweezers (nine molecules in each replica) were placed over the membranes at an initial distance of 4 Å following a previously reported protocol.[14] The tweezer−membrane systems were subjected to three production runs of 200 ns each of Gaussian accelerated Molecular Dynamics simulations (GaMD)[12] for a total of 600 ns sampling in explicit TIP3P water.[13] In the case of CP026, a similar setup as for CP024 and CP020 was used for 200 ns of GaMD. The simulations were performed using a 2 fs time step in a constant pressure regime of 1 bar at 300 K. For the long-range electrostatics, the particle-mesh Ewald method was employed.[14] A cutoff of 12 Å was used. The plane of the membrane was perpendicular to the *z*-axis. Harmonic restraints were then used to prevent the tweezers from artificially crossing the membranes in the +*z*-direction and to keep the lipids from leaving the membrane by diffusing in the same direction.[14] The GaMD simulations were performed using NAMD2.13 and NAMD3.0 alpha9 (NAMD was developed by the Theoretical and Computational Biophysics Group in the Beckman Institute for Advanced Science and Technology at the University of Illinois at Urbana-Champaign)[15] and the CHARMM36[16,17] force field. The parameters for the tweezers were obtained by using the Swissparam server.[18] Tweezer parameters obtained in this way have been tested and validated by us in previous work.[19,20] VMD 1.9.3[21] was used for visualization and analysis of the trajectories. For the analysis of the lipids tilt angles, MEMBPLUGIN was used.[22] For evaluating the tilt angles of the unbound lipids, we used the lower leaflet of the membrane. This way, no tweezer interacts with that leaflet since we imposed constraints on the *z*-position of the tweezers to avoid artificial crossing of the membranes. Thus, the tilt angles of the lipids bound to tweezers can be compared to that of the lipids alone, which are not affected by the influence of the tweezers, within the same simulation.

Liposome Dye Leakage

Liposomes were prepared and tweezers tested as previously described.[14]

https://doi.org/10.1021/jacsau.2c00220
JACS Au XXXX, XXX, XXX−XXX

SARS-CoV-2 Infection Experiment in Mice

Transgenic K18-hACE2 mice were obtained from a commercial supplier (Jackson Laboratory, USA) and bred at Fraunhofer IZI. Male mice (14 weeks old) were randomly assigned into groups of 6 animals and kept under standard conditions in isolated ventilated cages. The animal experiment was carried under BSL3 conditions and performed in accordance with the EU Directive 2010/63/EU for animal experiments and was approved by local authorities. For therapy, the tweezer molecules (CP019, CP025, or CP006) were mixed with 300 FFU SARS-CoV-2 wildtype (WT, BetaCoV/Germany/BavPat1/2020 p.1 strain) at a concentration of 150 μM/50 μL. After a 1 min incubation on 37 °C, the mixture was applied via intranasal route in 50 μL total volume under isoflurane anesthesia. The control group was infected with 300 FFU SARS-CoV-2 WT mixed with PBS. Seven hours after infection, the mice received a second treatment at the same doses. Mice were monitored daily for body weight and clinical score and euthanized on day 2 after virus inoculation. Lung tissues were collected in gentleMACS M tubes (Miltenyi Biotec, Germany) filled with 2 mL PBS on ice. The tissue was homogenized using gentleMACS Octo Dissociator (Miltenyi Biotec, Germany) with the RNA_1 program. Afterward, tissue homogenates were centrifuged at 2000×g for 5 min at 4 °C to separate cell debris and the supernatant was removed and stored at −80 °C until viral RNA isolation. Viral RNA was isolated from 140 μL of homogenate supernatants using QIAamp Viral RNA Mini Kit (Qiagen, Germany) according to manufacturer's instructions. RT-qPCR reactions were performed using TaqMan Fast Virus 1-Step Master Mix (Thermo Fisher) and 5 μL of isolated RNA as a template according to the published protocol.[23] Ten-fold serial dilutions in the range of 5×10^2 to 5×10^6 copies/5 μL of synthetic SARS-CoV-2-RNA (Twist Bioscience, USA) were used as a quantitative standard to obtain viral copy numbers. Statistical evaluation (Graph Pad Prism) of the data was performed by Kruskal–Wallis test (one-way ANOVA) and Dunn's Pairwise Multiple Comparison Procedures as *post hoc* test in comparison to the mock-treated control.

SDS PAGE and Immunoblotting

Murine lung homogenates as prepared for quantification of viral loads by qPCR were used for preparation of protein lysates for WB analysis. 10% (v/v) lysis buffer (10% Triton X-100, 10% SDS) and protein inhibitor cocktail were spiked into homogenates, followed by high speed vortexing for 30s and incubation at 4 °C for 5 min. Samples were then centrifuged at 21,000×g for 20 min, and supernatants transferred to new tubes as protein lysates. Protein concentrations were determined by BCA Assay (Pierce Rapid Gold BCA Protein Assay Kit, ThermoFisher) and adjusted to the sample with the lowest concentration with PBS to achieve equal loading. Loading dye (4× Protein Sample Loading Buffer, Licor; final concentration 1×) and reducing agent (TCEP, Sigma Aldrich, final concentration 50 mM) were added and samples heated to 70 °C for 10 min. An amount of 15 μg protein was loaded per lane on Novex BisTris 4–12% Gels and separated in MES buffer (200 V, 30 min). Proteins were transferred to PVDF membranes then blocked in Casein Blocker (ThermoFisher) for 1 h at RT. Membranes were incubated in primary AB (SARS-CoV-2-N: 40143-R001 SinoBio) overnight, washed 3× in PBS-Tween 20 (0.05%), and incubated with secondary StarBright 520-coupled anti-rabbit AB (Bio-Rad) and primary labeled anti-Tubulin hFAB Rhodamine-coupled (Bio-Rad) antibodies for 1 h RT. After 4× washing, membranes were imaged on a Bio-Rad ChemiDoc MP Imaging System. Intensity of bands was quantified by a Fiji's (ImageJ) built-in gel analysis tool.

RSV Infection Experiment in Mice

Female BALB/cJ mice were purchased from Charles River (Germany) at 8 weeks of age and maintained in a specific pathogen-free environment in isolated ventilated cages. All animal experiments were carried out in accordance with the EU Directive 2010/63/EU for animal experiments and were approved by local authorities (no.: TVV 42/17). Two groups of six mice received an intranasal (i.n.) treatment under isoflurane anesthesia of 100 nmol of either CLR01 or CLR03 mixed with 10^6 focus forming units (FFU) of purified RSV (the Long strain, obtained from ATCC) in 50 μL total volume. The third group served as a control and was infected intranasally with 10^6 FFU of RSV in 50 μL PBS. On day 5 post-infection, mice lungs were collected and homogenized using gentleMACS M Tubes (Miltenyi Biotec, Germany) containing 2 mL of ice-cold PBS using gentleMACS Dissociator (Miltenyi Biotec, Germany). Homogenized tissues were cleared of debris by centrifugation at 2000×g and 4 °C for 5 min. RNA was isolated from 140 μL of homogenate supernatants using the QIAamp-Viral-RNA-Mini Kit (Qiagen) according to the manufacturer's instructions. An amount of 45 ng of isolated RNA was reverse transcribed and analyzed with the QuantiTect probe RT-PCR kit (Qiagen) using an RSA-1 forward primer (5′-AGATCAACTTCTGTCATCCAGCAA-3′), an RSA-2 reverse primer (5′-GCACATCATAATTAGGAGTAT-CAAT-3′), and SYBR Green detection. Ten-fold dilutions of synthetic RSV-RNA of T7-transcripts were used as RNA standards for the quantification of RSV copy numbers in mouse samples as described.[24] Statistical analyses were performed using GraphPad Prism Software Version 6 and one-way ANOVA with the Kruskal–Wallis test and Dunn's Pairwise Multiple Comparison Procedures as *post hoc* test. Statistically significant differences are indicated as follows: * = p < 0.05, ** = p < 0.01, **** = p < 0.001, **** = p < 0.0001, ns = not significant.

Nonlinear Regression and Statistics

Unless stated otherwise, analysis was performed using GraphPad Prism version 9.0.1. Calculations of IC_{50} values via nonlinear regression were performed using the normalized response-variable slope equation. For statistical analysis, ordinary one-way ANOVA with Dunett's multiple comparison test was used. For correlation analysis, Spearman correlation was performed.

■ ASSOCIATED CONTENT

Supporting Information

The Supporting Information is available free of charge at https://pubs.acs.org/doi/10.1021/jacsau.2c00220.

(Movie 1) Tweezers inactivate SARS-CoV-2. A respective SARS-CoV-2/tweezer sample of the experiment shown in Figure 1 and Figure S2 was fixed after tweezer treatment, stained with uranyl acetate, and visualized by TEM in scanning transmission mode (MP4)

Material and methods, supplementary figures, supplementary tables, synthesis of the tweezers, and ^{1}H NMR and HR mass spectra of all new diester tweezers (PDF)

■ AUTHOR INFORMATION

Corresponding Authors

Elsa Sanchez-Garcia − *Computational Biochemistry, University of Duisburg-Essen, Essen 45117, Germany;* orcid.org/0000-0002-9211-5803; Email: elsa.sanchez-garcia@uni-due.de

Thomas Schrader − *Faculty of Chemistry, University of Duisburg-Essen, Essen 45117, Germany;* orcid.org/0000-0002-7003-6362; Email: thomas.schrader@uni-due.de

Jan Münch − *Institute of Molecular Virology, Ulm University Medical Center, Ulm 89081, Germany;* orcid.org/0000-0001-7316-7141; Email: jan.muench@uni-ulm.de

Authors

Tatjana Weil − *Institute of Molecular Virology, Ulm University Medical Center, Ulm 89081, Germany;* orcid.org/0000-0003-0925-2426

https://doi.org/10.1021/jacsau.2c00220
JACS Au XXXX, XXX, XXX−XXX

Abbna Kirupakaran − *Faculty of Chemistry, University of Duisburg-Essen, Essen 45117, Germany*
My-Hue Le − *Faculty of Chemistry, University of Duisburg-Essen, Essen 45117, Germany*
Philipp Rebmann − *Faculty of Chemistry, University of Duisburg-Essen, Essen 45117, Germany*
Joel Mieres-Perez − *Computational Biochemistry, University of Duisburg-Essen, Essen 45117, Germany*
Leila Issmail − *Fraunhofer Institute for Cell Therapy and Immunology IZI, Leipzig 04103, Germany*
Carina Conzelmann − *Institute of Molecular Virology, Ulm University Medical Center, Ulm 89081, Germany*
Janis A. Müller − *Institute of Virology, Philipps University of Marburg, Marburg 35043, Germany*
Lena Rauch − *Institute of Molecular Virology, Ulm University Medical Center, Ulm 89081, Germany*
Andrea Gilg − *Institute of Molecular Virology, Ulm University Medical Center, Ulm 89081, Germany*
Lukas Wettstein − *Institute of Molecular Virology, Ulm University Medical Center, Ulm 89081, Germany*
Rüdiger Groß − *Institute of Molecular Virology, Ulm University Medical Center, Ulm 89081, Germany;* orcid.org/0000-0003-0355-7915
Clarissa Read − *Central Facility for Electron Microscopy, Ulm University, Ulm 89081, Germany; Institute of Virology, Ulm University Medical Center, Ulm 89081, Germany*
Tim Bergner − *Central Facility for Electron Microscopy, Ulm University, Ulm 89081, Germany*
Sandra Axberg Pålsson − *Department of Molecular Biosciences, The Wenner-Gren Institute, Stockholm University, Stockholm 10691, Sweden*
Nadja Uhlig − *Fraunhofer Institute for Cell Therapy and Immunology IZI, Leipzig 04103, Germany;* orcid.org/0000-0002-7407-0955
Valentina Eberlein − *Fraunhofer Institute for Cell Therapy and Immunology IZI, Leipzig 04103, Germany*
Heike Wöll − *Faculty of Chemistry, University of Duisburg-Essen, Essen 45117, Germany*
Frank-Gerrit Klärner − *Faculty of Chemistry, University of Duisburg-Essen, Essen 45117, Germany*
Steffen Stenger − *Institute for Microbiology and Hygiene, Ulm University Medical Center, Ulm 89081, Germany*
Beate M. Kümmerer − *Institute of Virology, Medical Faculty, University of Bonn, Bonn 53127, Germany; German Centre for Infection Research (DZIF), Bonn 53127, Germany*
Hendrik Streeck − *Institute of Virology, Medical Faculty, University of Bonn, Bonn 53127, Germany; German Centre for Infection Research (DZIF), Bonn 53127, Germany*
Giorgio Fois − *Institute of General Physiology, Ulm University, Ulm 89081, Germany*
Manfred Frick − *Institute of General Physiology, Ulm University, Ulm 89081, Germany;* orcid.org/0000-0002-4763-1104
Peter Braubach − *Institute of Pathology, Hannover Medical School (MHH), Hannover 30625, Germany*
Anna-Lena Spetz − *Department of Molecular Biosciences, The Wenner-Gren Institute, Stockholm University, Stockholm 10691, Sweden*
Thomas Grunwald − *Fraunhofer Institute for Cell Therapy and Immunology IZI, Leipzig 04103, Germany*
James Shorter − *Department of Biochemistry and Biophysics, Perelman School of Medicine at the University of Pennsylvania, Philadelphia 19104, United States;* orcid.org/0000-0001-5269-8533

Complete contact information is available at: https://pubs.acs.org/10.1021/jacsau.2c00220

Author Contributions

°A.K., M.-H.L., and P.R. contributed equally to this work. T.W. generated SARS-CoV-2 and LV(Luc)-CoV-2 stocks and performed liposomes dye leakage assay, cytotoxicity assay, LV(Luc)-CoV-2 assay, HIV-1 assay and infection experiments in the BSL-3 with SARS-CoV-2. J.A.M. and C.C. also generated SARS-CoV-2 stocks and assisted T.W. with the infection assays with SARS-CoV-2. T.B. and C.R. performed TEM analysis. P.R., A.K., and M.-H.L. designed, synthesized, and characterized a new potent class of tweezers; F.-G.K. and T.S. developed the tweezer design; T.S. supervised all synthetic work and wrote part of the manuscript; J.M.-P. and E.S.-G. designed, performed, analyzed, and wrote the results of the computational modeling; L.W. generated L.V. pseudotypes and assisted T.W. with LV(Luc)-CoV-2 assays; A.G. generated and performed assays with MeV; L.R. generated and performed assays with IAV; S.A.P. generated and performed the RSV assay; J.M and T.G. designed the animal experiments; L.I. carried out RSV mice experiments; L.I., N.U. and V.E. carried out SARS-CoV-2 mice experiments; R.G. performed WB analysis; H.W performed the preparative HPLC purification of all compounds; S.S. supervised the BSL-3 work; A.S. supervised work with RSV; P.B. collected and provided HAECs; G.F. and M.F. differentiated and cultured HAECs and collected mucus; B.M.K. and H.S. isolated, propagated, and provided the Delta variant; and T.W., C.R., J.S., E.S.-G., T.S., and J.M. wrote and revised the manuscript.

Notes

The authors declare the following competing financial interest(s): T.S. and J.M. are inventors of a granted patent application that claims to use molecular tweezers as antiviral agents.
In memory of Carsten Schmuck.

■ ACKNOWLEDGMENTS

T.S. and J.M. acknowledge funding by the EU's Horizon 2020 research and innovation programme (Fight-nCoV, 101003555). This work was further supported by the German Research Foundation (DFG) through "Fokus-Förderung COVID-19" grants to J.M. (MU 3115-13), and the CRC 1279 to E.S.-G. and J.M. Generous support is gratefully acknowledged through the Collaborative Research Centre 1093 (CRC 1093) funded by the German Research Foundation (DFG), subprojects A03 (T.S.) and A08 (E.S.-G.). E.S.-G. was also supported by the DFG under Germany's Excellence Strategy−EXC 2033−390677874−RESOLV and by the DFG−Projektnummer: 436586093. E.S.-G. acknowledges the computational time provided at the supercomputer magnitUDE of the University of Duisburg-Essen. We thank Anna Eis-Hübinger for initial testing of the virus sample and Janett Wieseler and Johanna Heuser for technical support regarding the virus lineage B.1.617.2. L.W., C.C., T.W., L.R., and R.G. are part of the International Graduate School in Molecular Medicine Ulm. We would like to thank Nicola Schrott, Daniela Krnavek, Isabell Schulz, Diana Engberg, and Anne-Kathrin Donner for excellent technical assistance and

Alexandra Rockstroh and Jasmin Fertey for providing purified SARS-CoV-2 for animal experiments.

REFERENCES

(1) McCreary, E. K.; Angus, D. C. Efficacy of Remdesivir in COVID-19. *JAMA* **2020**, *324*, 1041−1042.
(2) EUA 105 Pfizer Paxlovid LOA (12222021) | Enhanced Reader moz-extension://d7e179ea-8b25−4590-95dc-ed847a8038e3/enhanced-reader.html?openApp&pdf=https%3A%2F%2Fwww.fda.gov%2Fmedia%2F155049%2Fdownload (accessed Jan 17, 2022).
(3) Zhao, J.; Cui, W.; Tian, B. P. Efficacy of Tocilizumab Treatment in Severely Ill COVID-19 Patients. *Crit. Care* **2020**, *24*, 1−4.
(4) Baden, L. R.; El Sahly, H. M.; Essink, B.; Kotloff, K.; Frey, S.; Novak, R.; Diemert, D.; Spector, S. A.; Rouphael, N.; Creech, C. B.; McGettigan, J.; Khetan, S.; Segall, N.; Solis, J.; Brosz, A.; Fierro, C.; Schwartz, H.; Neuzil, K.; Corey, L.; Gilbert, P.; Janes, H.; Follmann, D.; Marovich, M.; Mascola, J.; Polakowski, L.; Ledgerwood, J.; Graham, B. S.; Bennett, H.; Pajon, R.; Knightly, C.; Leav, B.; Deng, W.; Zhou, H.; Han, S.; Ivarsson, M.; Miller, J.; Zaks, T. Efficacy and Safety of the MRNA-1273 SARS-CoV-2 Vaccine. *N. Engl. J. Med.* **2021**, *384*, 403−416.
(5) Conzelmann, C.; Gilg, A.; Groß, R.; Schütz, D.; et al. An Enzyme-Based Immunodetection Assay to Quantify SARS-CoV-2 Infection. *Antiviral Res.* **2020**, *181*, 104882.
(6) Li, Q.; Nie, J.; Wu, J.; Zhang, L.; Ding, R.; Wang, H.; Zhang, Y.; Li, T.; Liu, S.; Zhang, M.; Zhao, C.; Liu, H.; Nie, L.; Qin, H.; Wang, M.; Lu, Q.; Li, X.; Liu, J.; Liang, H.; Shi, Y.; Shen, Y.; Xie, L.; Zhang, L.; Qu, X.; Xu, W.; Huang, W.; Wang, Y. SARS-CoV-2 501Y.V2 Variants Lack Higher Infectivity but Do Have Immune Escape. *Cell* **2021**, *184*, 2362−2371.
(7) Möller, L.; Schünadel, L.; Nitsche, A.; Schwebke, I.; Hanisch, M.; Laue, M. Evaluation of Virus Inactivation by Formaldehyde to Enhance Biosafety of Diagnostic Electron Microscopy. *Viruses* **2015**, *7* (2), 666−679.
(8) Laue, M. Electron Microscopy of Viruses. *Methods Cell Biol.* **2010**, *96*.
(9) Kremer, J. R.; Mastronarde, D. N.; McIntosh, J. R. Computer Visualization of Three-Dimensional Image Data Using IMOD. *J. Struct. Biol.* **1996**, *116* (1), 71−76.
(10) Grint, D. J.; Wing, K.; Williamson, E.; McDonald, H. I.; Bhaskaran, K.; Evans, D.; Evans, S. J.; Walker, A. J.; Hickman, G.; Nightingale, E.; Schultze, A.; Rentsch, C. T.; Bates, C.; Cockburn, J.; Curtis, H. J.; Morton, C. E.; Bacon, S.; Davy, S.; Wong, A. Y.; Mehrkar, A.; Tomlinson, L.; Douglas, I. J.; Mathur, R.; Blomquist, P.; MacKenna, B.; Ingelsby, P.; Croker, R.; Parry, J.; Hester, F.; Harper, S.; DeVito, N. J.; Hulme, W.; Tazare, J.; Goldacre, B.; Smeeth, L.; Eggo, R. M. Case Fatality Risk of the SARS-CoV-2 Variant of Concern B.1.1.7 in England, 16 November to 5 February. *Eurosurveillance* **2021**, *26*, 2100256.
(11) Davies, N. G.; Jarvis, C. I.; van Zandvoort, K.; Clifford, S.; Sun, F. Y.; Funk, S.; Medley, G.; Jafari, Y.; Meakin, S. R.; Lowe, R.; Quaife, M.; Waterlow, N. R.; Eggo, R. M.; Lei, J.; Koltai, M.; Krauer, F.; Tully, D. C.; Munday, J. D.; Showering, A.; Foss, A. M.; Prem, K.; Flasche, S.; Kucharski, A. J.; Abbott, S.; Quilty, B. J.; Jombart, T.; Rosello, A.; Knight, G. M.; Jit, M.; Liu, Y.; Williams, J.; Hellewell, J.; O'Reilly, K.; Chan, Y. W. D.; Russell, T. W.; Procter, S. R.; Endo, A.; Nightingale, E. S.; Bosse, N. I.; Villabona-Arenas, C. J.; Sandmann, F. G.; Gimma, A.; Abbas, K.; Waites, W.; Atkins, K. E.; Barnard, R. C.; Klepac, P.; Gibbs, H. P.; Pearson, C. A. B.; Brady, O.; Edmunds, W. J.; Jewell, N. P.; Diaz-Ordaz, K.; Keogh, R. H. Increased Mortality in Community-Tested Cases of SARS-CoV-2 Lineage B.1.1.7. *Nature* **2021**, *593*, 270−274.
(12) Pang, Y. T.; Miao, Y.; Wang, Y.; McCammon, J. A. Gaussian Accelerated Molecular Dynamics in NAMD. *J. Chem. Theory Comput.* **2017**, *13* (1), 9−19.
(13) Jorgensen, W. L.; Chandrasekhar, J.; Madura, J. D.; Impey, R. W.; Klein, M. L. Comparison of Simple Potential Functions for Simulating Liquid Water. *J. Chem. Phys.* **1983**, *79* (2), 926−935.
(14) Darden, T.; York, D.; Pedersen, L. Particle Mesh Ewald: An *N*·log(N) Method for Ewald Sums in Large Systems. *J. Chem. Phys.* **1993**, *98* (12), 10089−10092.
(15) Phillips, J. C.; Braun, R.; Wang, W.; Gumbart, J.; Tajkhorshid, E.; Chipot, C.; Skeel, R. D.; Kalé, L.; Schulten, J. Scalable Molecular Dynamics with NAMD. Journal of Computational Chemistry. Wiley Subscription Services, Inc., A Wiley Company, 2005; pp 1781−1802.
(16) Vanommeslaeghe, K.; Mackerell, A. D. CHARMM Additive and Polarizable Force Fields for Biophysics and Computer-Aided Drug Design. In *Biochimica et Biophysica Acta - General Subjects*. Elsevier B.V. 2015, pp 861−871.
(17) Klauda, J. B.; Venable, R. M.; Freites, J. A.; O'Connor, J. W.; Tobias, D. J.; et al. Update of the CHARMM All-Atom Additive Force Field for Lipids: Validation on Six Lipid Types. *J. Phys. Chem. B* **2010**, *114* (23), 7830−7843.
(18) Zoete, V.; Cuendet, M. A.; Grosdidier, A.; Michielin, O. SwissParam: A Fast Force Field Generation Tool for Small Organic Molecules. *J. Comput. Chem.* **2011**, *32* (11), 2359−2368.
(19) Bier, D.; Rose, R.; Bravo-Rodriguez, K.; Bartel, M.; et al. Molecular Tweezers Modulate 14-3-3 Protein−Protein Interactions. *Nat. Chem.* **2013**, *5* (3), 234−239.
(20) Lump, E.; Castellano, L. M.; Meier, C.; Seeliger, J.; et al. Molecular Tweezers Modulate 14-3-3 Protein−Protein Interactions. *Elife* **2015**, *4*, 1−33.
(21) Humphrey, W.; Dalke, A.; Schulten, K Molecular Tweezers Modulate 14-3-3 Protein−Protein Interactions. *J. Mol. Graph.* **1996**, *14* (1), 33−38.
(22) Guixà-González, R.; Rodriguez-Espigares, I.; Ramírez-Anguita, J. M.; Carrió-Gaspar, P.; et al. MEMBPLUGIN: Studying Membrane Complexity in VMD. *Bioinformatics* **2014**, *30* (10), 1478−1480.
(23) Groß, R.; Conzelmann, C.; Müller, J. A.; Stenger, S.; et al. Detection of SARS-Co-V-2 in Human Breastmilk. The Lancet. Lancet Publishing Group, 2020; pp 1757−1758.
(24) Kohlmann, R.; Schwannecke, S.; Tippler, B.; Ternette, N.; et al. Protective Efficacy and Immunogenecity of an Adenoviral Vector Vaccine Encoding the Codon-Optimized F Protein of Respiratory Syncytial Virus. *J. Virol.* **2009**, *83* (23), 12601−12610.
(25) Klein, S.; Cortese, M.; Winter, S. L.; Wachsmuth-Melm, M.; Neufeldt, C. J.; Cerikan, B.; Stanifer, M. L.; Boulant, S.; Bartenschlager, R.; Chlanda, P. SARS-CoV-2 Structure and Replication Characterized by in Situ Cryo-Electron Tomography. *Nat. Commun.* **2020**, *11*, 1−10.
(26) Fokkens, M.; Schrader, T.; Klärner, F. G. A Molecular Tweezer for Lysine and Arginine. *J. Am. Chem. Soc.* **2005**, *127*, 14415−14421.
(27) Bergwerk, M.; Gonen, T.; Lustig, Y.; Amit, S.; Lipsitch, M.; Cohen, C.; Mandelboim, M.; Gal Levin, E.; Rubin, C.; Indenbaum, V.; Tal, I.; Zavitan, M.; Zuckerman, N.; Bar-Chaim, A.; Kreiss, Y.; Regev-Yochay, G. Covid-19 Breakthrough Infections in Vaccinated Health Care Workers. *N. Engl. J. Med.* **2021**, *385*, 1474−1484.
(28) Brown, C. M.; Vostok, J.; Johnson, H.; Burns, M.; Gharpure, R.; Sami, S.; Sabo, R. T.; Hall, N.; Foreman, A.; Schubert, P. L.; Gallagher, G. R.; Fink, T.; Madoff, L. C.; Gabriel, S. B.; MacInnis, B.; Park, D. J.; Siddle, K. J.; Harik, V.; Arvidson, D.; Brock-Fisher, T.; Dunn, M.; Kearns, A.; Laney, A. S. Outbreak of SARS-CoV-2 Infections, Including COVID-19 Vaccine Breakthrough Infections, Associated with Large Public Gatherings—Barnstable County, Massachusetts, July 2021. *Morb. Mortal. Wkly. Rep.* **2021**, *70*, 1059−1062.
(29) Corey, L.; Beyrer, C.; Cohen, M. S.; Michael, N. L.; Bedford, T.; Rolland, M. SARS-CoV-2 Variants in Patients with Immunosuppression. *N. Engl. J. Med.* **2021**, *385*, 562−566.
(30) Riemersma, K. K.; Grogan, B. E.; Kita-Yarbro, A.; Halfmann, P.; Kocharian, A.; Florek, K. R.; Westergaard, R.; Bateman, A.; Jeppson, G. E.; Kawaoka, Y.; O'connor, D. H.; Friedrich, T. C.; Grande, K. M. Shedding of Infectious SARS-CoV-2 Despite Vaccination When the Delta Variant Is Prevalent - Wisconsin, July 2021. *MedRXiv* **2021**, DOI: 10.1101/2021.07.31.21261387.
(31) Hoffmann, M.; Krüger, N.; Schulz, S.; Cossmann, A.; Rocha, C.; Kempf, A.; Nehlmeier, I.; Graichen, L.; Moldenhauer, A.-S.;

https://doi.org/10.1021/jacsau.2c00220
JACS Au XXXX, XXX, XXX−XXX

Winkler, M. S.; Lier, M.; Dopfer-Jablonka, A.; Jäck, H.-M.; Behrens, G. M. N.; Pöhlmann, S. The Omicron Variant Is Highly Resistant against Antibody-Mediated Neutralization: Implications for Control of the COVID-19 Pandemic. *Cell* **2022**, *185*, 447−456.

https://doi.org/10.1021/jacsau.2c00220
JACS Au XXXX, XXX, XXX−XXX